



Research article

Study on modeling and dynamic performance of a planar flexible parallel manipulator based on finite element method

Zhen Liu^{1,*}, Song Yang¹, Chen Cheng¹, Tao Ding¹ and Ruimin Chai²

¹ Xi'an Research Inst. of Hi-Tech, Xi'an 710025, China

² Xi'an North Electro-Optic Science and Technology Defense Co., Ltd., Xi'an 710043, China

* **Correspondence:** Email: liuzhen_029@163.com.

Abstract: The application of a high-speed parallel manipulator necessitates the adoption of a lightweight design to reduce dead weight. However, this increases the elastic deformation of certain components, affecting the dynamic performance of the system. This study examined a 2-DOF planar flexible parallel manipulator. A dynamic model of the parallel manipulator composed of fully flexible links was established using a floating reference coordinate system and a combination of the finite element and augmented Lagrange multiplier methods. A dynamic analysis of the simplified model under three driving torque modes showed that the axial deformation was less than the transverse deformation by three orders of magnitude. Further, the kinematic and dynamic performance of the redundant drive was significantly better than that of the non-redundant drive, and the vibration was well suppressed in the redundant drive mode. In addition, the comprehensive performance of driving Mode 2 was better than that of the other two modes. Finally, the validity of the dynamic model was verified by modeling via Adams. The modular modeling method is conducive to the extension to other models and programming. Furthermore, the dynamic model of the established fully flexible link system can aid in optimizing the lightweight design and dynamic performance of the parallel manipulator.

Keywords: parallel manipulator; redundant actuation; finite element method; flexible body; dynamic modeling

1. Introduction

Compared with serial manipulators, parallel manipulators offer the benefits of large stiffness, excellent dynamic performance, and small cumulative error [1]. With the rapid technological development in recent years, they are being widely used in motion simulation, aeronautical manufacturing, high-speed machining, medicine, and other fields [2–6]. However, it suffers from certain disadvantages such as a small workspace with many singularities and the difficulty in solving dynamics problems.

The singularity of the parallel manipulator can result in motion instability and the decline of stiffness and accuracy. Therefore, the design and application of parallel manipulators should avoid singularities as far as possible, particularly the second type. Numerous studies conducted on this subject have proposed certain methods to avoid singularities [7–10]. Specifically, the drive redundancy method [4,11] can effectively avoid singularities without increasing the degree of freedom (DOF) of the system.

To adapt to the working environment of high-speed motion in certain applications, the parallel manipulator frequently adopts a lightweight design. However, certain components may experience flexible deformation with the accumulation of the high-speed motion of the manipulator movement with time. Consequently, the dynamic performance and motion accuracy of the entire system is affected. In recent years, many studies have focused on the dynamic modeling of flexible parallel manipulators. Liang et al. studied a 2-DOF multi-drive parallel manipulator, established a rigid-flexible coupling dynamic model, and conducted control research [12,13]. Chen et al. studied a 3-RRR parallel manipulator, established a rigid-flexible coupling dynamic model, and conducted dynamic research [14]. Rosyid et al. studied a 3-PRR asymmetric planar parallel manipulator and established a rigid-flexible coupling dynamic model [15]. Sheng et al. established a rigid-flexible coupling dynamic model of a parallel manipulator with flexible intermediate links and verified it via modal analysis [16].

In addition, there are many scholars who have carried out many meaningful studies on the control strategy of flexible parallel robots [17–20], which are of great significance for improving the accuracy of trajectory tracking and positioning of flexible parallel robots.

Owing to the modeling being based on a flexible multi-body system, the final result is generally a complex time-variant nonlinear partial differential equation. Thus, obtaining the analytical solution for complex flexible systems is challenging. Generally, the flexible body is discretized to reduce the complexity of the research, primarily through the following methods: 1) finite element method (FEM) [21,22], 2) assumed mode method (AMM) [23,24], 3) finite segment method (FSM) [25], and 4) lumped parameter method [26]; FEM and AMM have been used extensively. A study compared these methods, and the results were found to be similar [27]. However, FEM can be applied to the flexible members with complex shapes. More accurate system dynamics model can be obtained when the elements are reasonably divided; therefore, the method is suitable for the dynamic analysis of the system. In contrast, AMM is more suitable for the study of active control.

Shang et al. studied a 3-RRR parallel manipulator [28], established the kinematics and rigid body dynamics models, and studied the control strategy. However, this study did not consider the influence of elastic deformation of components on the dynamic performance of the entire system when the manipulator was in high-speed motion.

Compared with the previous work, this paper adopts the floating reference coordinate system and finite element method, combined with the augmented Lagrange multiplier method, to establish a

dynamic model of the parallel robot composed of fully flexible Levers, and analyzes the dynamic performance of the simplified model in three driving modes. The modeling adopts a modular approach, which is conducive to generalizing to other models and is more conducive to programming, and the dynamic model of the fully flexible Lever system established is conducive to the optimization between the lightweight design and dynamic performance of the parallel robot, and also helps the subsequent control strategy research.

This study examined a 3-RRR flexible parallel manipulator. To facilitate modeling, a floating reference coordinate system was used to describe the deformed body. The methodology of the study conducted is as follows: In Section 2, The 3-RRR parallel mechanism was described. In Section 3, FEM was used to discretize a single flexible body and establish the dynamic equation of the module. The dynamic equation of a single flexible body was obtained by assembling the module. Further, the flexible bodies were assembled to obtain the dynamic equation of the open chain system. Subsequently, the constraint equation was established and combined with the dynamics equation of the open chain system to form a complete system dynamics equation. In Section 4, the driving torques in three different modes obtained from the inverse dynamics of the rigid body were used as feed-forward input, and the dynamic response was obtained using the ode23tb solver. In Section 5, the numerical simulation results were compared with Adams software simulation results to verify the correctness of the model. In Section 6, finally, certain conclusions were drawn from the results obtained.

2. Model overview

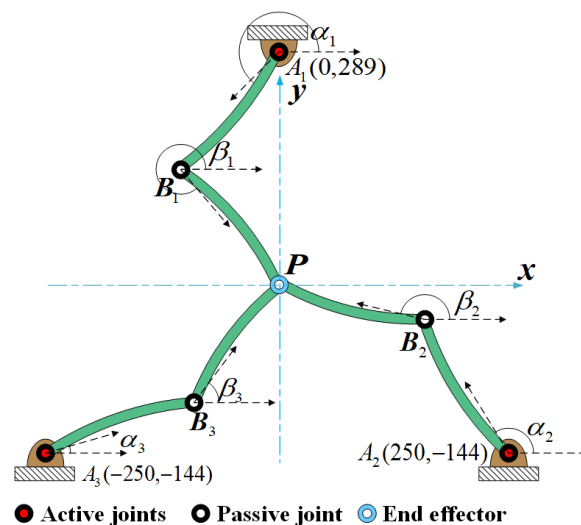


Figure 1. Flexible deformation of 3-RRR parallel manipulator in motion.

Figure 1 shows the structure of the 3-RRR parallel manipulator. Specifically, A_i is the position of the active joint of the i^{th} branch chain, whose coordinates are marked as (x_{A_i}, y_{A_i}) and angle as α_i ; B_i is the position of slave joint of the i^{th} branch chain, whose coordinates are marked as (x_{B_i}, y_{B_i}) and angle as β_i ; the position of the end-effector is marked as P and its coordinates as (x_p, y_p) ; and the coordinates of the active joint are $A_1(0, 289)$, $A_2(250, -144)$ and $A_3(-250, -144)$. A redundant parallel manipulator is formed when A_1 , A_2 and A_3 function as the driving joint, and a non-redundant parallel manipulator formed when A_1 and A_2 function as the driving joint.

3. Dynamics modeling of rigid-flexible coupling system

To improve their dynamic performance, parallel manipulators often adopt a lightweight design, which results in the deformation of certain components when the manipulator works at high speed. Consequently, the dynamic performance of the manipulator is affected. Therefore, certain components of the manipulator must be flexible and a rigid-flexible coupling dynamic model needs to be established.

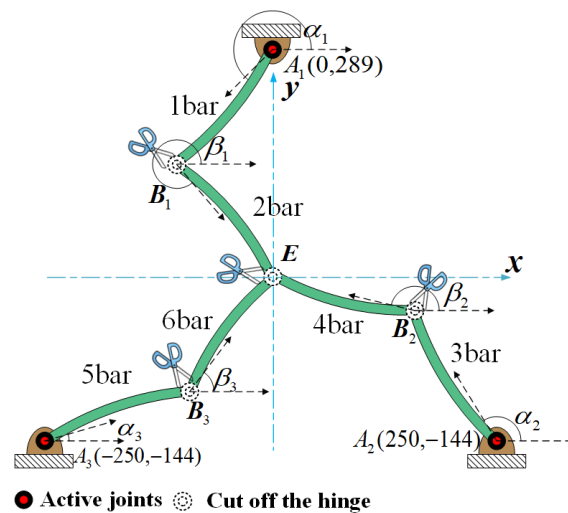


Figure 2. Schematic of 3-RRR parallel manipulator hinge uncoupling.

To facilitate the modeling, first, the slave joint and end effector were disconnected, as shown in Figure 2, to form an independent flexible body. Subsequently, the dynamics equation of each independent flexible body was derived. Finally, various parts were assembled to form a complete system dynamics equation.

3.1. Dynamics equation of single flexible body j

For the convenience of description, all levers were numbered uniformly as j ($j = 1, 2, \dots, 6$). As the section size of the lever was much smaller than the length of the lever, the Euler–Bernoulli beam theory was applied.

This study employed the floating reference coordinate system to describe the deformed body; that is, the motion of the flexible body was divided into two parts: elastic deformation in the body-connected coordinate system and large-scale motion of the entire body-connected coordinate system relative to the inertial reference system, as shown in Figure 3. In this figure, $O-x-y$ is the global coordinate system of the system where the rack is located, $O_j-x'-y'$ is the flexible body-connected coordinate system, P is any point along the axis of the body-connected coordinate system, r_{O_j} is the radius vector of the origin of the body-connected coordinate system in the global coordinate system, $r_{O_j, P} = [x' \ 0]^T$ is the radius vector in the body-connected coordinate system $O_j-x'-y'$ of any point P on the flexible body j before deformation, $\delta_p = [u_j \ v_j]^T$ expresses the deformation displacement

vector from P or P' in the body-connected coordinate system, and \mathbf{r}_p is the position vector of the position P' of the deformed flexible body in the global coordinate system.

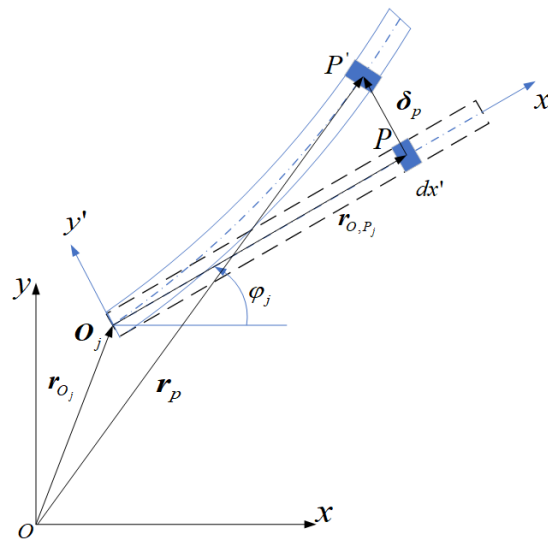


Figure 3. Deformation of any flexible body j in motion.

According to the closed vector relationship shown in Figure 3, the following equation is obtained:

$$\mathbf{r}_{Pi}^j = \mathbf{r}_{O_j} + \mathbf{R}(\varphi_j)(\mathbf{r}_{O,P_j} + \delta_p), \quad (1)$$

where $\mathbf{R}(\varphi_j) = \begin{bmatrix} \cos \varphi_j & -\sin \varphi_j \\ \sin \varphi_j & \cos \varphi_j \end{bmatrix}$ is the rotation transformation matrix of the body-connected coordinate system relative to the global coordinate system, and φ_j is the rotational angular displacement of the flexible body j .

3.1.1. Discretization of flexible body j

FEM was used to discretize the flexible body j . For this purpose, the beam element was selected, each containing the left and right nodes and each node containing three generalized coordinates [29], as shown in Figure 4.

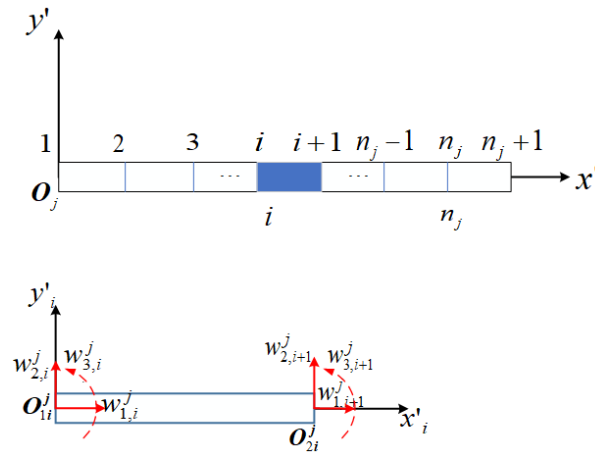


Figure 4. Discretization of finite element of arbitrary flexible body j and one element i .

Here, $O'_i - x'_i - y'_i$ is the coordinate system of the module i , $w_{1,i}^j$, $w_{2,i}^j$ and $w_{3,i}^j$ represent the axial elastic displacement, transverse elastic displacement, and elastic rotational angle of the node i , respectively. The generalized coordinate array of the flexible element i is expressed as:

$$\mathbf{w}_i^j = [w_{1,i}^j \quad w_{2,i}^j \quad w_{3,i}^j \quad w_{1,i+1}^j \quad w_{2,i+1}^j \quad w_{3,i+1}^j]^T. \quad (2)$$

The deformation displacement vector of any point P_i^j on the element i in the flexible body j in the element coordinate system is expressed as:

$$\boldsymbol{\delta}_{P_i^j} = \begin{bmatrix} u_i^j(x'_i, t) \\ v_i^j(x'_i, t) \end{bmatrix} = \mathbf{S}_i^j(x'_i) \mathbf{w}_i^j, \quad (3)$$

where $\mathbf{S}_i^j(x'_i)$ is the type function matrix of the element i , given by:

$$\mathbf{S}_i^j(x'_i) = \begin{bmatrix} \mathbf{S}_{i,1}^j(x'_i) \\ \mathbf{S}_{i,2}^j(x'_i) \end{bmatrix} = \begin{bmatrix} N_{i,1}^j & 0 & 0 & N_{i+1,1}^j & 0 & 0 \\ 0 & N_{i,2}^j & N_{i,3}^j & 0 & N_{i+1,2}^j & N_{i+1,3}^j \end{bmatrix}, \quad (4)$$

where $N_{i,1}^j = 1 - \frac{x'_i}{l_i^j}$, $N_{i,2}^j = 1 - 3\left(\frac{x'_i}{l_i^j}\right)^2 + 2\left(\frac{x'_i}{l_i^j}\right)^3$, $N_{i,3}^j = l_i^j \left[\frac{x'_i}{l_i^j} - 2\left(\frac{x'_i}{l_i^j}\right)^2 + \left(\frac{x'_i}{l_i^j}\right)^3 \right]$, $N_{i+1,1}^j = \frac{x'_i}{l_i^j}$,

$N_{i+1,2}^j = 3\left(\frac{x'_i}{l_i^j}\right)^2 - 2\left(\frac{x'_i}{l_i^j}\right)^3$, and $N_{i+1,3}^j = l_i^j \left[\left(\frac{x'_i}{l_i^j}\right)^3 - \left(\frac{x'_i}{l_i^j}\right)^2 \right]$. Specifically, l_i^j is the length of the

element i in the flexible body j without deformation.

Overall deformation displacement array of flexible body j is expressed as:

$$\mathbf{W}^j = [w_{1,1}^j \quad w_{2,1}^j \quad w_{3,1}^j \quad \cdots \quad w_{1,n_j+1}^j \quad w_{2,n_j+1}^j \quad w_{3,n_j+1}^j]_{3(n_j+1) \times 1}^T. \quad (5)$$

After discretizing the flexible body j via FEM, the displacement vector of any point P_i^j on its

upper element i in the global coordinate system after deformation is

$$\mathbf{r}_{p_i}^j = \mathbf{r}_{O_j} + \mathbf{R}^j(\varphi_j)(\mathbf{r}_{O,i}^j + \mathbf{S}_i^j(x'_i)\mathbf{B}_i^j \underbrace{\mathbf{D}^j \mathbf{w}^j}_{\mathbf{W}^j}), \quad (6)$$

where $\mathbf{r}_{O,i}^j = \left[\sum_{k=0}^{i-1} \mathbf{l}_k^j + \mathbf{x}'_i \quad 0 \right]^T$ ($\mathbf{l}_0^j = 0$) is the coordinate array of any point P_i^j on the element i of the flexible body j in the body-connected coordinate system before the deformation, and \mathbf{B}_i^j is the Boolean indicator matrix of the element i in the flexible body j .

$$\mathbf{B}_i^j = \begin{bmatrix} \mathbf{0}_{3 \times 3} & \mathbf{0}_{3 \times 3} & \cdots & \mathbf{I}_{3 \times 3} & \mathbf{0}_{3 \times 3} & \cdots & \mathbf{0}_{3 \times 3} & \mathbf{0}_{3 \times 3} \\ \mathbf{0}_{3 \times 3} & \mathbf{0}_{3 \times 3} & \cdots & \mathbf{0}_{3 \times 3} & \mathbf{I}_{3 \times 3} & \cdots & \mathbf{0}_{3 \times 3} & \mathbf{0}_{3 \times 3} \end{bmatrix}_{6 \times 3(n_j+1)}. \quad (7)$$

For the cantilever beam model, the axial and transverse elastic displacements and elastic rotation at the first node are zero according to its boundary conditions. Then, the independent overall deformation displacement array of the flexible body j is expressed as:

$$\mathbf{w}^j = [w_{1,2}^j \quad w_{2,2}^j \quad w_{3,2}^j \quad \cdots \quad w_{1,n+1}^j \quad w_{2,n+1}^j \quad w_{3,n+1}^j]. \quad (8)$$

Thus, the corresponding global generalized coordinate transformation matrix can be written as:

$$\mathbf{D}^j = \begin{bmatrix} \mathbf{0}_{3 \times 3n_j} \\ \mathbf{I}_{3n_j \times 3n_j} \end{bmatrix}_{3(n_j+1) \times 3n_j}. \quad (9)$$

The generalized coordinate array j of an arbitrary flexible body is defined as:

$$\mathbf{q}_j = [\mathbf{r}_{O_j}^T \quad \varphi_j \quad \mathbf{w}^{jT}]^T. \quad (10)$$

To solve the first derivative of time for closed vector Eq (6), the following is considered:

$$\dot{\mathbf{r}}_{p_i}^j = \dot{\mathbf{r}}_{O_j} + \frac{\partial \mathbf{R}^j(\varphi_j)}{\partial \varphi_j} \dot{\varphi}_j (\mathbf{r}_{O,i}^j + \mathbf{S}_i^j(x'_i)\mathbf{B}_i^j \mathbf{D}^j \mathbf{w}^j) + \mathbf{R}(\varphi_j) \mathbf{S}_i^j(x'_i) \mathbf{B}_i^j \mathbf{D}^j \dot{\mathbf{w}}^j. \quad (11)$$

To facilitate the subsequent calculation, it is transformed into the form of matrix

$$\dot{\mathbf{r}}_{p_i}^j = \mathbf{H}_i^j \dot{\mathbf{q}}_j, \quad (12)$$

$$\mathbf{H}_i^j = \begin{bmatrix} \mathbf{I}_{2 \times 2} & \frac{\partial \mathbf{R}^j(\varphi_j)}{\partial \varphi_j} \dot{\varphi}_j (\mathbf{r}_{O,i}^j + \mathbf{S}_i^j(x'_i)\mathbf{B}_i^j \mathbf{D}^j \mathbf{w}^j) & \mathbf{R}(\varphi_j) \mathbf{S}_i^j(x'_i) \mathbf{B}_i^j \mathbf{D}^j \dot{\mathbf{w}}^j \end{bmatrix}_{2 \times (3+3n_j)} \quad (13)$$

3.1.2. Dynamics modeling of arbitrary element i

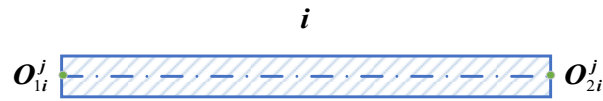


Figure 5. Beam element i .

A beam element i as shown in Figure 5. According to the results of kinematic analysis, the kinetic energy of the element i can be expressed as:

$$T_i^j = \frac{1}{2} \int_{V_i^j} \rho \dot{\mathbf{r}}_{p_i}^{jT} \dot{\mathbf{r}}_{p_i}^j dV_i^j = \frac{1}{2} \int_{V_i^j} \rho \dot{\mathbf{q}}_j^T \mathbf{H}_i^{vjT} \mathbf{H}_i^{vj} \dot{\mathbf{q}}_j dV_i^j = \frac{1}{2} \dot{\mathbf{q}}_j^T \mathbf{M}_i^j \dot{\mathbf{q}}_j. \quad (14)$$

The mass matrix corresponding to the volume \mathbf{M}_i^j of the middle continuum of the element V_i^j , with the material density of ρ , is a symmetric positive definite matrix as follows:

$$\mathbf{M}_i^j = \int_{V_i^j} \rho \mathbf{H}_i^{vjT} \mathbf{H}_i^{vj} dV_i^j, \quad (15)$$

$$\mathbf{M}_i^j = \begin{bmatrix} \mathbf{M}_{i,rr}^j & \mathbf{M}_{i,r\varphi}^j & \mathbf{M}_{i,rf}^j \\ \mathbf{M}_{i,\varphi r}^j & \mathbf{M}_{i,\varphi\varphi}^j & \mathbf{M}_{i,\varphi f}^j \\ \mathbf{M}_{i,fr}^j & \mathbf{M}_{i,f\varphi}^j & \mathbf{M}_{i,ff}^j \end{bmatrix}. \quad (16)$$

To facilitate the subsequent calculation, several commonly used integrals are expressed as follows:

$$\mathbf{G}_{i,1}^j = \int_{V_i^j} \rho \mathbf{r}_{O,i}^j dV_i^j,$$

$$\mathbf{G}_{i,2}^j = \int_{V_i^j} \rho \mathbf{S}_i^j(x'_i) \mathbf{B}_i^j \mathbf{D}^j dV_i^j,$$

$$\tilde{\mathbf{k}} = \begin{bmatrix} 0 & 1 \\ -1 & 0 \end{bmatrix},$$

potential energy analysis of arbitrary element i is determined as follows: Since the 3-RRR workspace is on the $O-x-y$ plane, the influence of gravity can be ignored. Here, only the bending strain energy and tensile and compressible strain energies of the element are considered, while the shear strain energy and buckling strain energy are ignored.

The strain energy of arbitrary element i in the flexible body j is as follows:

$$U_{p,i}^j = \frac{1}{2} \int_0^{l_i^j} EI \left(\frac{\partial^2 v_i^j(x'_i, t)}{\partial x_i'^2} \right)^2 dx'_i + \frac{1}{2} \int_0^{l_i^j} EA \left(\frac{\partial u_i^j(x'_i, t)}{\partial x_i'} \right)^2 dx'_i = \frac{1}{2} \mathbf{q}_j^T \mathbf{K}_i^j \mathbf{q}_j, \quad (17)$$

where E is the elastic modulus of the material, I is the cross-sectional moment of inertia of the element, A is the cross-sectional area of the beam element, and \mathbf{K}_i^j is the stiffness matrix of the beam element,

$$\mathbf{K}_i^j = \begin{bmatrix} \mathbf{0}_{2 \times 2} & \mathbf{0}_{2 \times 1} & \mathbf{0}_{2 \times 3n_j} \\ \mathbf{0}_{1 \times 2} & 0 & \mathbf{0}_{1 \times 3n_j} \\ \mathbf{0}_{3n_j \times 2} & \mathbf{0}_{3n_j \times 1} & \mathbf{K}_{i,ff}^j \end{bmatrix}, \quad (18)$$

where

$$\begin{aligned} \mathbf{K}_{i,ff}^j &= \int_0^{l_i^j} EID^{jT} \mathbf{B}_i^{jT} \left(\frac{\partial^2 \mathbf{G}_{i,2}^j(x'_i)}{\partial x_i'^2} \right)^T \left(\frac{\partial^2 \mathbf{G}_{i,2}^j(x'_i)}{\partial x_i'^2} \right) \mathbf{B}_i^j \mathbf{D}^j dx'_i + \\ &\int_0^{l_i^j} EAD^{jT} \mathbf{B}_i^{jT} \left(\frac{\partial \mathbf{G}_{i,1}^j(x'_i)}{\partial x'_i} \right)^T \left(\frac{\partial \mathbf{G}_{i,1}^j(x'_i)}{\partial x'_i} \right) \mathbf{B}_i^j \mathbf{D}^j dx'_i \end{aligned}$$

Dynamics equation of arbitrary element i is determined as follows: Considering the kinetic and potential energies of the element into the Lagrange equation, the following is obtained:

$$\frac{d}{dt} \left(\frac{\partial \zeta_i^j}{\partial \dot{\mathbf{q}}_j} \right) - \frac{\partial \zeta_i^j}{\partial \mathbf{q}_j} = \mathbf{F}_{e,i}^j, \quad (19)$$

where $\mathbf{F}_{e,i}^j$ is the generalized external force array of elements, and ζ_i^j is the Lagrange function.

$$\zeta_i^j = T_i^j - U_{p,i}^j = \frac{1}{2} \dot{\mathbf{q}}_j^T \mathbf{M}_i^j \dot{\mathbf{q}}_j - \frac{1}{2} \dot{\mathbf{q}}_j^T \mathbf{K}_i^j \dot{\mathbf{q}}_j$$

Further, on rearranging the elements in Eq (19):

$$\frac{\partial \zeta_i^j}{\partial \mathbf{q}_j} = \frac{\partial \left(\frac{1}{2} \dot{\mathbf{q}}_j^T \mathbf{M}_i^j \dot{\mathbf{q}}_j \right)}{\partial \mathbf{q}_j} - \mathbf{K}_i^j \mathbf{q}_j = \frac{1}{2} (\mathbf{I} \otimes \dot{\mathbf{q}}_j)^T \frac{\partial \mathbf{M}_i^j}{\partial \mathbf{q}_j} \dot{\mathbf{q}}_j = \mathbf{C}_{i2}^j \dot{\mathbf{q}}_j, \quad (20)$$

$$\frac{d}{dt} \left(\frac{\partial \zeta_i^j}{\partial \dot{\mathbf{q}}_j} \right) = \frac{d}{dt} (\mathbf{M}_i^j \dot{\mathbf{q}}_j) = \frac{d\mathbf{M}_i^j}{dt} \dot{\mathbf{q}}_j + \mathbf{M}_i^j \ddot{\mathbf{q}}_j, \quad (21)$$

where

$$\frac{d\mathbf{M}_i^j}{dt} \dot{\mathbf{q}}_j = \frac{\partial \mathbf{M}_i^j}{\partial \mathbf{q}_j^T} \dot{\mathbf{q}}_j^T \dot{\mathbf{q}}_j = \frac{\partial \mathbf{M}_i^j}{\partial \mathbf{q}_j^T} (\dot{\mathbf{q}}_j \otimes \mathbf{I}) \dot{\mathbf{q}}_j = \mathbf{C}_{i1}^j \dot{\mathbf{q}}_j. \quad (22)$$

Through further rearrangement of Eq (19), the following is obtained:

$$\mathbf{M}_i^j \ddot{\mathbf{q}}_j + \mathbf{C}_i^j \dot{\mathbf{q}}_j + \mathbf{K}_i^j \mathbf{q}_j = \mathbf{F}_{e,i}^j, \quad (23)$$

where

$$\mathbf{C}_i^j = \mathbf{C}_{i1}^j - \mathbf{C}_{i2}^j = \frac{\partial \mathbf{M}_i^j}{\partial \mathbf{q}_j^T} (\dot{\mathbf{q}}_j \otimes \mathbf{I}) - \frac{1}{2} (\mathbf{I} \otimes \dot{\mathbf{q}}_j)^T \frac{\partial \mathbf{M}_i^j}{\partial \mathbf{q}_j}, \quad (24)$$

where symbol \otimes indicates the Kronecker product, and \mathbf{I}_{3n+3} indicates the unit diagonal matrix.

$$\mathbf{C}_i^j = \begin{bmatrix} \mathbf{C}_{i,rr}^j & \mathbf{C}_{i,r\varphi}^j & \mathbf{C}_{i,rf}^j \\ \mathbf{C}_{i,\varphi r}^j & \mathbf{C}_{i,\varphi\varphi}^j & \mathbf{C}_{i,\varphi f}^j \\ \mathbf{C}_{i,fr}^j & \mathbf{C}_{i,f\varphi}^j & \mathbf{C}_{i,ff}^j \end{bmatrix}.$$

Thus far, the mass, stiffness, and centrifugal force/Coriolis force matrices of the dynamics Eq (23) of any element i on the flexible body j have been obtained, and the dynamics equation modeling of the module i has been completed.

3.1.3. Dynamics equation of arbitrary flexible body j

As the dynamics Eq (23) of the element i is established in the generalized coordinate system of the flexible body j , the dynamics equation of the flexible body j can be obtained provided the dynamics equations of all the elements i in the flexible body j are accumulated.

$$\mathbf{M}^j \ddot{\mathbf{q}}_j + \mathbf{C}^j \dot{\mathbf{q}}_j + \mathbf{K}^j \mathbf{q}_j = \mathbf{F}^j, \quad (25)$$

where

$$\mathbf{M}_j = \sum_{i=1}^{n_j} \mathbf{M}_i^j, \quad \mathbf{C}_j = \sum_{i=1}^{n_j} \mathbf{C}_i^j, \quad \mathbf{K}_j = \sum_{i=1}^{n_j} \mathbf{K}_i^j, \quad \mathbf{F}_j = \sum_{i=1}^{n_j} \mathbf{F}_{e,i}^j.$$

Here, n_j is the number of discretized elements in the flexible body j . To facilitate discussion, the discretization number of all flexible bodies was considered same in the subsequent sections; that is $n_j = n (j = 1, \dots, 6)$.

3.2. Modeling of system dynamics equation

3.2.1. System dynamics equation without constraints

First, the system dynamics equation without constraints is established. The mechanism is composed of six flexible bodies. The generalized coordinate array of the system is written as

$$\mathbf{q}^{(s)} = [\mathbf{r}_{O_1}^T \quad \varphi_1 \quad \mathbf{w}^{1T} \quad \dots \quad \mathbf{r}_{O_6}^T \quad \varphi_6 \quad \mathbf{w}^{6T}]. \quad (26)$$

By assembling the six flexible bodies, the system dynamics equations without constraints can be established as:

$$\mathbf{M}^{(s)} \ddot{\mathbf{q}}^{(s)} + \mathbf{C}^{(s)} \dot{\mathbf{q}}^{(s)} + \mathbf{K}^{(s)} \mathbf{q}^{(s)} = \mathbf{F}_e^{(s)}, \quad (27)$$

where

$$\mathbf{M}^{(s)} = \text{diag}(\mathbf{M}_1 \quad \mathbf{M}_2 \quad \dots \quad \mathbf{M}_6), \quad \mathbf{C}^{(s)} = \text{diag}(\mathbf{C}_1 \quad \mathbf{C}_2 \quad \dots \quad \mathbf{C}_6),$$

$$\mathbf{K}^{(s)} = \text{diag}(\mathbf{K}_1 \quad \mathbf{K}_2 \quad \cdots \quad \mathbf{K}_6), \quad \mathbf{F}_e^{(s)} = \text{diag}(\mathbf{F}_{e,1}^T \quad \mathbf{F}_{e,2}^T \quad \cdots \quad \mathbf{F}_{e,6}^T)^T.$$

3.2.2. Constraint equation of the system

To establish a complete system dynamics equation, certain constraints must be imposed on the joints and disconnected joints of the end effector based on the system dynamics equation without constraints. The constraints include the joint position and link constraints, totaling 18 constraint equations. The specific equations are as follows:

Position coordinate constraint equation:

$$\text{Joint } A_1 \quad \boldsymbol{\Psi}_1 \stackrel{\Delta}{=} \mathbf{r}_{A_1} - \begin{bmatrix} x_{A_1} \\ y_{A_1} \end{bmatrix} = \mathbf{0}_{2 \times 1}, \quad (28)$$

$$\text{Joint } A_2 \quad \boldsymbol{\Psi}_2 \stackrel{\Delta}{=} \mathbf{r}_{A_2} - \begin{bmatrix} x_{A_2} \\ y_{A_2} \end{bmatrix} = \mathbf{0}_{2 \times 1}, \quad (29)$$

$$\text{Joint } A_3 \quad \boldsymbol{\Psi}_3 \stackrel{\Delta}{=} \mathbf{r}_{A_3} - \begin{bmatrix} x_{A_3} \\ y_{A_3} \end{bmatrix} = \mathbf{0}_{2 \times 1}, \quad (30)$$

$$\text{Joint } B_1 \quad \boldsymbol{\Psi}_4 \stackrel{\Delta}{=} \mathbf{r}_{B_1} - \begin{bmatrix} x_{A_1} \\ y_{A_1} \end{bmatrix} - \mathbf{R}(\varphi_1) \begin{bmatrix} l_1 + w_{1,x'}^{end} \\ w_{1,y'}^{end} \end{bmatrix} = \mathbf{0}_{2 \times 1}, \quad (31)$$

$$\text{Joint } B_2 \quad \boldsymbol{\Psi}_5 \stackrel{\Delta}{=} \mathbf{r}_{B_2} - \begin{bmatrix} x_{A_2} \\ y_{A_2} \end{bmatrix} - \mathbf{R}(\varphi_3) \begin{bmatrix} l_1 + w_{3,x'}^{end} \\ w_{3,y'}^{end} \end{bmatrix} = \mathbf{0}_{2 \times 1}, \quad (32)$$

$$\text{Joint } B_3 \quad \boldsymbol{\Psi}_6 \stackrel{\Delta}{=} \mathbf{r}_{B_3} - \begin{bmatrix} x_{A_3} \\ y_{A_3} \end{bmatrix} - \mathbf{R}(\varphi_5) \begin{bmatrix} l_1 + w_{5,x'}^{end} \\ w_{5,y'}^{end} \end{bmatrix} = \mathbf{0}_{2 \times 1}, \quad (33)$$

Link constraint equation:

$$\text{Branch chain 1} \quad \boldsymbol{\Psi}_7 \stackrel{\Delta}{=} \begin{bmatrix} x_{A_1} \\ y_{A_1} \end{bmatrix} + \mathbf{R}(\varphi_1) \begin{bmatrix} l_1 + w_{1,x'}^{end} \\ w_{1,y'}^{end} \end{bmatrix} + \mathbf{R}(\varphi_2) \begin{bmatrix} l_2 + w_{2,x'}^{end} \\ w_{2,y'}^{end} \end{bmatrix} - \begin{bmatrix} x_P \\ y_P \end{bmatrix} = \mathbf{0}_{2 \times 1}, \quad (34)$$

$$\text{Branch chain 2} \quad \boldsymbol{\Psi}_8 \stackrel{\Delta}{=} \begin{bmatrix} x_{A_2} \\ y_{A_2} \end{bmatrix} + \mathbf{R}(\varphi_3) \begin{bmatrix} l_1 + w_{3,x'}^{end} \\ w_{3,y'}^{end} \end{bmatrix} + \mathbf{R}(\varphi_4) \begin{bmatrix} l_2 + w_{4,x'}^{end} \\ w_{4,y'}^{end} \end{bmatrix} - \begin{bmatrix} x_P \\ y_P \end{bmatrix} = \mathbf{0}_{2 \times 1}, \quad (35)$$

$$\text{Branch chain 3} \quad \boldsymbol{\Psi}_9 \stackrel{\Delta}{=} \begin{bmatrix} x_{A_3} \\ y_{A_3} \end{bmatrix} + \mathbf{R}(\varphi_5) \begin{bmatrix} l_1 + w_{5,x'}^{end} \\ w_{5,y'}^{end} \end{bmatrix} + \mathbf{R}(\varphi_6) \begin{bmatrix} l_2 + w_{6,x'}^{end} \\ w_{6,y'}^{end} \end{bmatrix} - \begin{bmatrix} x_P \\ y_P \end{bmatrix} = \mathbf{0}_{2 \times 1}, \quad (36)$$

where $\mathbf{q}_P = [x_P \quad y_P]^T$ is the coordinates of the end effector.

The constraint equation of the system is written as:

$$\boldsymbol{\Psi}(\mathbf{q}^{(s)}, t) = \mathbf{0}_{18 \times 1}, \quad (37)$$

where $\Psi(\mathbf{q}^{(s)}, t) = [\psi_1^T \ \psi_2^T \ \dots \ \psi_9^T]^T \in R^{18}$.

To facilitate the operation, the generalized variable array (26) is reorganized into the following form

$$\tilde{\mathbf{q}}^{(s)} = \left[\underbrace{\mathbf{r}_{O_1}^T \ \dots \ \mathbf{r}_{O_6}^T}_{\mathbf{q}_r} \quad \underbrace{\varphi_1 \ \dots \ \varphi_6}_{\mathbf{q}_\varphi} \quad \underbrace{\mathbf{w}^{1T} \ \dots \ \mathbf{w}^{6T}}_{\mathbf{q}_w} \right]_{(18n+18) \times 1}^T. \quad (38)$$

The mapping between $\mathbf{q}^{(s)}$ and $\tilde{\mathbf{q}}^{(s)}$ can be expressed as:

$$\mathbf{q}^{(s)} = \zeta \tilde{\mathbf{q}}^{(s)}, \quad (39)$$

where ζ is the adjustment matrix between $\mathbf{q}^{(s)}$ and $\tilde{\mathbf{q}}^{(s)}$.

$$\zeta = [\zeta_1^T \ \zeta_2^T \ \zeta_3^T \ \zeta_4^T \ \zeta_5^T \ \zeta_6^T]^T, \quad (40)$$

$$\text{where } \zeta_j = \begin{bmatrix} \mathbf{0}_{2 \times 2(j-1)} & \mathbf{I}_{2 \times 2} & \mathbf{0}_{2 \times (18+6n-2j)} \\ \mathbf{0}_{1 \times (j+1)} & \mathbf{I}_{1 \times 1} & \mathbf{0}_{1 \times (6+6n-j)} \\ \mathbf{0}_{n \times (nj-n+18)} & \mathbf{I}_{n \times n} & \mathbf{0}_{n \times n(6-j)} \end{bmatrix} \quad (j = 1, \dots, 6)$$

Solving the first derivative of time for Eq (37), the following is obtained:

$$\mathbf{J}_q(\mathbf{q}^{(s)}, t) \dot{\mathbf{q}}^{(s)} + \boldsymbol{\psi}_t = \mathbf{0}_{18 \times 1}, \quad (41)$$

where $\mathbf{J}_q(\mathbf{q}^{(s)}, t) = \frac{\partial \Psi(\mathbf{q}^{(s)}, t)}{\partial \mathbf{q}^{(s)T}}$ is the system constraint Jacobian matrix. As the constraint equation is time independent, therefore $\boldsymbol{\psi}_t = \frac{\partial \Psi(\mathbf{q}^{(s)}, t)}{\partial t} = \mathbf{0}_{18 \times 1}$. Thus, it can be concluded that

$$\mathbf{J}_q(\mathbf{q}^{(s)}, t) \dot{\mathbf{q}}^{(s)} = \mathbf{0}_{18 \times 1}. \quad (42)$$

According to Eq (26), the first derivative of the generalized coordinates of the system can be expressed as:

$$\dot{\mathbf{q}}^{(s)} = [\dot{\mathbf{r}}_{O_1}^T \ \dot{\varphi}_1 \ \dot{\mathbf{w}}^{1T} \ \dots \ \dot{\mathbf{r}}_{O_6}^T \ \dot{\varphi}_6 \ \dot{\mathbf{w}}^{6T}]^T. \quad (43)$$

The second derivative of the generalized coordinates of the system can be expressed as:

$$\ddot{\mathbf{q}}^{(s)} = [\ddot{\mathbf{r}}_{O_1}^T \ \ddot{\varphi}_1 \ \ddot{\mathbf{w}}^{1T} \ \dots \ \ddot{\mathbf{r}}_{O_6}^T \ \ddot{\varphi}_6 \ \ddot{\mathbf{w}}^{6T}]^T. \quad (44)$$

Subsequently, while determining the second derivative of time for Eq (37), the following equation is obtained:

$$\mathbf{J}_q(\mathbf{q}^{(s)}, t)\ddot{\mathbf{q}}^{(s)} = \boldsymbol{\eta}, \quad (45)$$

where,

$$\boldsymbol{\eta} = -\frac{\partial}{\partial \mathbf{q}^{(s)T}} \left(\frac{\partial \boldsymbol{\psi}(\mathbf{q}^{(s)}, t)}{\partial \mathbf{q}^{(s)T}} \dot{\mathbf{q}}^{(s)} \right) \dot{\mathbf{q}}^{(s)} - 2 \frac{\partial}{\partial t} \left(\frac{\partial \boldsymbol{\psi}(\mathbf{q}^{(s)}, t)}{\partial \mathbf{q}^{(s)T}} \right) \dot{\mathbf{q}}^{(s)} - \frac{\partial^2 \boldsymbol{\psi}(\mathbf{q}^{(s)}, t)}{\partial t^2}. \quad (46)$$

3.2.3. Complete system dynamics equation

By combining the open-chain system Eq (27) with the constraint Eq (37) and introducing Lagrange multipliers, a complete system dynamics equation can be obtained as follows:

$$\begin{cases} \mathbf{M}^{(s)}\ddot{\mathbf{q}}^{(s)} + \mathbf{C}^{(s)}\dot{\mathbf{q}}^{(s)} + \mathbf{K}^{(s)}\mathbf{q}^{(s)} + \mathbf{J}_q^T(\mathbf{q}^{(s)}, t)\boldsymbol{\lambda} = \mathbf{F}_e^{(s)}, \\ \boldsymbol{\psi}(\mathbf{q}^{(s)}, t) = \mathbf{0}_{18 \times 1} \end{cases}, \quad (47)$$

where $\boldsymbol{\lambda} \in \mathbb{R}^{18}$ is the Lagrange multiplier array.

$$\mathbf{F}_e^{(s)} = \begin{bmatrix} \underbrace{\mathbf{0}_{1 \times 2} \quad \tau_1 \quad \mathbf{0}_{1 \times 3n_1}}_{\text{Flexible body 1}} & \underbrace{\mathbf{0}_{1 \times (3n_2+3)}}_{\text{Flexible body 2}} & \underbrace{\mathbf{0}_{1 \times 2} \quad \tau_3 \quad \mathbf{0}_{1 \times 3n_3}}_{\text{Flexible body 3}} & \underbrace{\mathbf{0}_{1 \times (3n_4+3)}}_{\text{Flexible body 4}} \\ \underbrace{\mathbf{0}_{1 \times 2} \quad \tau_5 \quad \mathbf{0}_{1 \times 3n_5}}_{\text{Flexible body 5}} & \underbrace{\mathbf{0}_{1 \times (3n_6+3)}}_{\text{Flexible body 6}} \end{bmatrix}^T. \quad (48)$$

The generalized independent coordinates of the system can be marked as:

$$\mathbf{q} = \begin{bmatrix} x_p & y_p & \mathbf{w}^{1T} & \dots & \mathbf{w}^{6T} \\ \mathbf{q}_p & & \mathbf{q}_w & & \end{bmatrix}_{(18n+2) \times 1}^T. \quad (49)$$

To ease the calculation, the constraint Eq (37) is expressed as

$$\boldsymbol{\psi}_1 \cdots \boldsymbol{\psi}_6 \stackrel{\Delta}{=} \boldsymbol{\psi}_a(\mathbf{q}_r, \mathbf{q}_\varphi, \mathbf{q}_w) = \mathbf{0}, \quad (50)$$

$$\boldsymbol{\psi}_7 \cdots \boldsymbol{\psi}_9 \stackrel{\Delta}{=} \boldsymbol{\psi}_b(\mathbf{q}_p, \mathbf{q}_\varphi, \mathbf{q}_w) = \mathbf{0}. \quad (51)$$

By solving the first derivative with respect to time at both ends of Eq (50), the following equation is obtained:

$$\dot{\boldsymbol{\psi}}_a \stackrel{\Delta}{=} \frac{\partial \boldsymbol{\psi}_a}{\partial \mathbf{q}_r^T} \dot{\mathbf{q}}_r + \frac{\partial \boldsymbol{\psi}_a}{\partial \mathbf{q}_\varphi^T} \dot{\mathbf{q}}_\varphi + \frac{\partial \boldsymbol{\psi}_a}{\partial \mathbf{q}_w^T} \dot{\mathbf{q}}_w = \mathbf{0}, \quad (52)$$

where $\partial \boldsymbol{\psi}_a / \partial \mathbf{q}_r^T$ is the 12th order reversible square matrix. By rearranging Eq (52), the following equation is obtained:

$$\dot{\mathbf{q}}_r = -\left(\frac{\partial \psi_a}{\partial \mathbf{q}_r^T}\right)^{-1} \frac{\partial \psi_a}{\partial \mathbf{q}_\varphi^T} \dot{\mathbf{q}}_\varphi - \left(\frac{\partial \psi_a}{\partial \mathbf{q}_r^T}\right)^{-1} \frac{\partial \psi_a}{\partial \mathbf{q}_w^T} \dot{\mathbf{q}}_w. \quad (53)$$

Further, by solving the first derivative with respect to time at both ends of Eq (51), the following equation is obtained:

$$\dot{\psi}_b \stackrel{\Delta}{=} \frac{\partial \psi_b}{\partial \mathbf{q}_\varphi^T} \dot{\mathbf{q}}_\varphi + \frac{\partial \psi_b}{\partial \mathbf{q}_w^T} \dot{\mathbf{q}}_w - \mathbf{Z} \dot{\mathbf{q}}_P = 0, \quad (54)$$

where $\mathbf{Z} = [\mathbf{I}_2 \quad \mathbf{I}_2 \quad \mathbf{I}_2]^T$, \mathbf{I}_2 is the identity matrix, and $\partial \psi_b / \partial \mathbf{q}_\varphi^T$ is a 6th order reversible square matrix. Eq (54) can be rearranged as:

$$\dot{\mathbf{q}}_\varphi = \left[\left(\frac{\partial \psi_b}{\partial \mathbf{q}_\varphi^T} \right)^{-1} \mathbf{Z} \quad - \left(\frac{\partial \psi_b}{\partial \mathbf{q}_\varphi^T} \right)^{-1} \frac{\partial \psi_b}{\partial \mathbf{q}_w^T} \right] \begin{bmatrix} \dot{\mathbf{q}}_P \\ \dot{\mathbf{q}}_w \end{bmatrix}. \quad (55)$$

For simplification, it is expressed as follows:

$$\mathbf{J}_{b\varphi} = \frac{\partial \psi_b}{\partial \mathbf{q}_\varphi^T}, \quad \mathbf{J}_{bw} = \frac{\partial \psi_b}{\partial \mathbf{q}_w^T}, \quad \mathbf{J}_{ar} = \frac{\partial \psi_a}{\partial \mathbf{q}_r^T}, \quad \mathbf{J}_{a\varphi} = \frac{\partial \psi_a}{\partial \mathbf{q}_\varphi^T}, \quad \mathbf{J}_{aw} = \frac{\partial \psi_a}{\partial \mathbf{q}_w^T}. \quad (56)$$

Substituting Eq (55) into Eq (53) and canceling $\dot{\mathbf{q}}_\varphi$,

$$\dot{\mathbf{q}}_r = [\Phi_1 \quad \Phi_2] \begin{bmatrix} \dot{\mathbf{q}}_P \\ \dot{\mathbf{q}}_w \end{bmatrix} = \Phi \begin{bmatrix} \dot{\mathbf{q}}_P \\ \dot{\mathbf{q}}_w \end{bmatrix}, \quad (57)$$

where,

$$\Phi_1 = -(\mathbf{J}_{ar})^{-1} \mathbf{J}_{a\varphi} (\mathbf{J}_{b\varphi})^{-1} \mathbf{Z}, \quad (58)$$

$$\Phi_2 = (\mathbf{J}_{ar})^{-1} \mathbf{J}_{a\varphi} (\mathbf{J}_{b\varphi})^{-1} \mathbf{J}_{bw} - (\mathbf{J}_{ar})^{-1} \mathbf{J}_{aw}, \quad (59)$$

$$\dot{\mathbf{q}}_\varphi = [\Gamma_1 \quad \Gamma_2] \begin{bmatrix} \dot{\mathbf{q}}_P \\ \dot{\mathbf{q}}_w \end{bmatrix} = \Gamma \begin{bmatrix} \dot{\mathbf{q}}_P \\ \dot{\mathbf{q}}_w \end{bmatrix}, \quad (60)$$

further,

$$\Gamma_1 = (\mathbf{J}_{b\varphi})^{-1} \mathbf{Z}, \quad (61)$$

$$\Gamma_2 = -(\mathbf{J}_{b\varphi})^{-1} \mathbf{J}_{bw}, \quad (62)$$

$$\dot{\mathbf{q}}_w = \mathbf{U} \begin{bmatrix} \dot{\mathbf{q}}_P \\ \dot{\mathbf{q}}_w \end{bmatrix}, \quad (63)$$

where, $\mathbf{U} = [\mathbf{0}_{18n \times 2} \quad \mathbf{I}_{18n \times 18n}]$.

By combining Eqs. (58), (61) and (64) with the generalized coordinate variable array (38), the

following is obtained:

$$\ddot{\tilde{q}}^{(s)} = \begin{bmatrix} \dot{q}_r \\ \dot{q}_\varphi \\ \dot{q}_w \end{bmatrix} = \Theta \begin{bmatrix} \dot{q}_P \\ \dot{q}_w \end{bmatrix} = \Theta \dot{q}, \quad (64)$$

where,

$$\Theta = \begin{bmatrix} \Phi_{12 \times (18n+2)} \\ \Gamma_{6 \times (18n+2)} \\ U_{18n \times (18n+2)} \end{bmatrix}. \quad (65)$$

This is the first-order mapping matrix between the generalized independent coordinate array and generalized coordinate variable array.

Further, solving the first-order derivative of time for Eq (65), the following equation is obtained:

$$\ddot{\tilde{q}}^{(s)} = \dot{\Theta} \dot{q} + \Theta \ddot{q}, \quad (66)$$

where,

$$\dot{\Theta} = \begin{bmatrix} \dot{\Phi} \\ \dot{\Gamma} \\ \dot{U} \end{bmatrix}. \quad (67)$$

Each element in Eq (68) can be expressed as:

$$\dot{\Phi} = \begin{bmatrix} \dot{\Phi}_1 & \dot{\Phi}_2 \end{bmatrix}, \quad (68)$$

$$\dot{\Gamma} = \begin{bmatrix} \dot{\Gamma}_1 & \dot{\Gamma}_2 \end{bmatrix}, \quad (69)$$

$$\dot{U} = \mathbf{0}_{18n \times (18n+2)}. \quad (70)$$

The mapping relationship between the independent generalized coordinate variable array (49) and generalized coordinate variable array (38) is

$$\tilde{q}^{(s)} = \Theta' q, \quad (71)$$

where,

$$\Theta' = \begin{bmatrix} \mathbf{0}_{18 \times 2} & \mathbf{0}_{18 \times 18n} \\ \mathbf{0}_{18n \times 2} & \mathbf{I}_{18n \times 18n} \end{bmatrix}. \quad (72)$$

To facilitate the calculation, the following settings are made

$$\begin{aligned}
\mathbf{j}_{ar} &= \left[\frac{\partial^2 \psi_a}{\partial (q_{r1})^2} \dot{q}_{r1} \quad \frac{\partial^2 \psi_a}{\partial (q_{r2})^2} \dot{q}_{r2} \quad \cdots \quad \frac{\partial^2 \psi_a}{\partial (q_{r12})^2} \dot{q}_{r12} \right], \\
\mathbf{j}_{b\phi} &= \left[\frac{\partial^2 \psi_b}{\partial (q_{\phi1})^2} \dot{q}_{\phi1} \quad \frac{\partial^2 \psi_b}{\partial (q_{\phi2})^2} \dot{q}_{\phi2} \quad \cdots \quad \frac{\partial^2 \psi_b}{\partial (q_{\phi6})^2} \dot{q}_{\phi6} \right], \\
\mathbf{j}_{bw} &= \left[\frac{\partial^2 \Psi_b}{\partial (q_{w1})^2} \dot{q}_{w1} \quad \frac{\partial^2 \Psi_b}{\partial (q_{w2})^2} \dot{q}_{w2} \quad \cdots \quad \frac{\partial^2 \Psi_b}{\partial (q_{w18n})^2} \dot{q}_{w18n} \right], \\
\mathbf{j}_{a\phi} &= \left[\frac{\partial^2 \Psi_a}{\partial (q_{\phi1})^2} \dot{q}_{\phi1} \quad \frac{\partial^2 \Psi_a}{\partial (q_{\phi2})^2} \dot{q}_{\phi2} \quad \cdots \quad \frac{\partial^2 \Psi_a}{\partial (q_{\phi6})^2} \dot{q}_{\phi6} \right], \\
\mathbf{j}_{aw} &= \left[\frac{\partial^2 \Psi_a}{\partial (q_{w1})^2} \dot{q}_{w1} \quad \frac{\partial^2 \Psi_a}{\partial (q_{w2})^2} \dot{q}_{w2} \quad \cdots \quad \frac{\partial^2 \Psi_a}{\partial (q_{w18n})^2} \dot{q}_{w18n} \right].
\end{aligned} \tag{73}$$

Thus far, the mapping relationship between the generalized coordinate variable array and system independent generalized coordinate array (including the first-order form and second-order form) is established.

$$\begin{cases} \mathbf{q}^{(s)} = \zeta \tilde{\mathbf{q}}^{(s)} = \zeta \Theta \mathbf{q} \\ \dot{\mathbf{q}}^{(s)} = \dot{\zeta} \tilde{\mathbf{q}}^{(s)} = \zeta \Theta \dot{\mathbf{q}} \\ \ddot{\mathbf{q}}^{(s)} = \ddot{\zeta} \tilde{\mathbf{q}}^{(s)} = \zeta \dot{\Theta} \dot{\mathbf{q}} + \zeta \Theta \ddot{\mathbf{q}} \end{cases}. \tag{74}$$

Substituting Eq (75) into constraint Eq (43) and combining the relationship between $\mathbf{q}^{(s)}$ and $\tilde{\mathbf{q}}^{(s)}$, the following relation is obtained:

$$\mathbf{J}_q(\mathbf{q}^{(s)}, t) \zeta \Theta \dot{\mathbf{q}} \equiv \mathbf{0}. \tag{75}$$

As \mathbf{q} is a generalized independent coordinate array of the system, the following relationship is always true for any \mathbf{q} in the system workspace:

$$\mathbf{J}_q(\mathbf{q}^{(s)}, t) \zeta \Theta \equiv \mathbf{0} \Leftrightarrow (\zeta \Theta)^T \mathbf{J}_q^T(\mathbf{q}^{(s)}, t) \equiv \mathbf{0}. \tag{76}$$

To eliminate the generalized constraining force $\mathbf{J}_q^T(\mathbf{q}^{(s)}, t) \lambda$ that is difficult to obtain in the closed-chain system equation, the two ends of the closed-chain system dynamics Eq (48) are multiplied by $(\zeta \Theta)^T$, and $(\zeta \Theta)^T \mathbf{J}_q^T(\mathbf{q}^{(s)}, t) \lambda$ is canceled. Thus, the following equation is obtained:

$$(\zeta \Theta)^T \mathbf{M}^{(s)} \ddot{\mathbf{q}}^{(s)} + (\zeta \Theta)^T \mathbf{C}^{(s)} \dot{\mathbf{q}}^{(s)} + (\zeta \Theta)^T \mathbf{K}^{(s)} \mathbf{q}^{(s)} = (\zeta \Theta)^T \mathbf{F}_e^{(s)}. \tag{77}$$

The mapping relationship (75) is plugged into Eq (78) and rearranged to obtain the complete dynamics equation of the system represented by the generalized independent coordinates of the system,

$$\mathbf{M} \ddot{\mathbf{q}} + \mathbf{C} \dot{\mathbf{q}} + \mathbf{K} \mathbf{q} = \mathbf{F}, \tag{78}$$

where,

$$\begin{aligned}
\mathbf{M} &= (\zeta \Theta)^T \mathbf{M}^{(s)} \zeta \Theta, \\
\mathbf{C} &= (\zeta \Theta)^T \mathbf{M}^{(s)} \dot{\zeta} \Theta + (\zeta \Theta)^T \mathbf{C}^{(s)} \zeta \Theta,
\end{aligned}$$

$$\mathbf{K} = (\zeta \Theta)^T \mathbf{K}^{(s)} \zeta \Theta,$$

$$\mathbf{F} = (\zeta \Theta)^T \mathbf{F}_e^{(s)}.$$

This completes the dynamics modeling.

4. Numerical simulation and analysis

To establish a generic dynamic model and facilitate the rigid-flexible coupling dynamic analysis, 1–6 levers are all considered flexible. The study found that the elastic deformation of the driving lever is more evident than that of the follower lever. Thus, to reduce the difficulty of numerical solution, only 1, 3 and 5 levers were considered flexible, and each lever was divided into three sections. Whereas, 2, 4 and 6 levers were regarded as rigid bodies. When the manipulator moves at high speed, its motion essentially includes two parts: large-scale rigid and small-scale flexible motions, which affect each other. The ode23tb solver was used to solve the system dynamics Eq (79) established in the previous section.

In this simulation, the planning path was that the center point P of the terminal console moved from the point (0,0) to the point (−14.42 mm, 36.15 mm) with a spiral trajectory within 0–0.5 s. The trajectory, velocity, and acceleration of point P are shown in Figures 6 and 7. The eccentric spiral was selected owing to the increasing speed and acceleration of the spiral trajectory, which is convenient for dynamic analysis. In addition, the influence of the asymmetric trajectory of eccentric spiral on the system was studied.

The parameters of a group of 3-RRR parallel manipulators are listed in Table 1. It was assumed that all the levers and terminal consoles were composed of aluminum with uniform texture, and all joints were light ideal bearings (i.e., massless, frictionless, clearanceless, etc.).

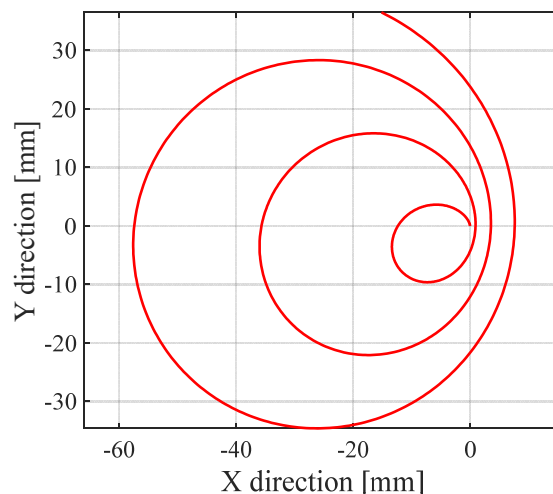


Figure 6. Trajectory of Point P.

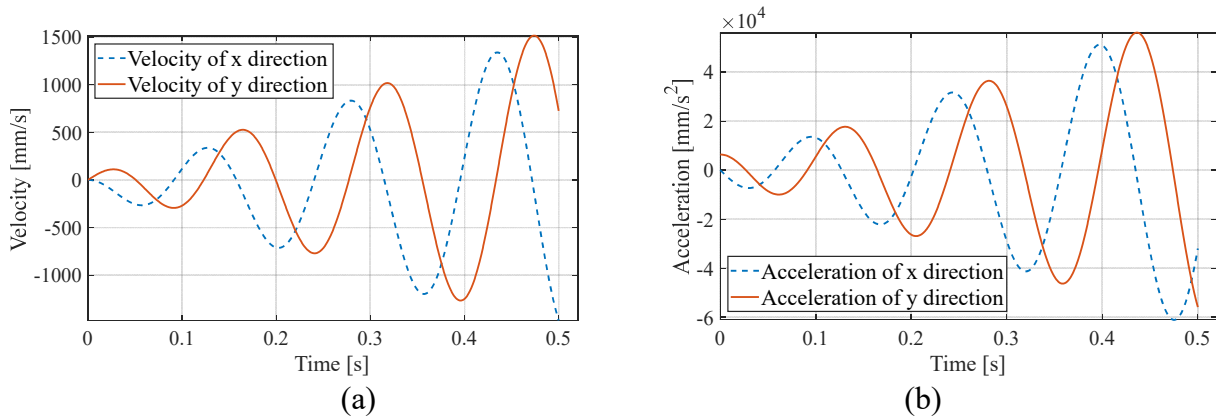


Figure 7. (a) P velocity of end-effector; (b) P acceleration of end-effector.

Table 1. Parameters of 3-RRR parallel manipulator (unit: mm).

l_1	l_2	Section A(mm ²)	Lever thickness h	ρ (g/mm ³)
244	244	40	5	0.0027

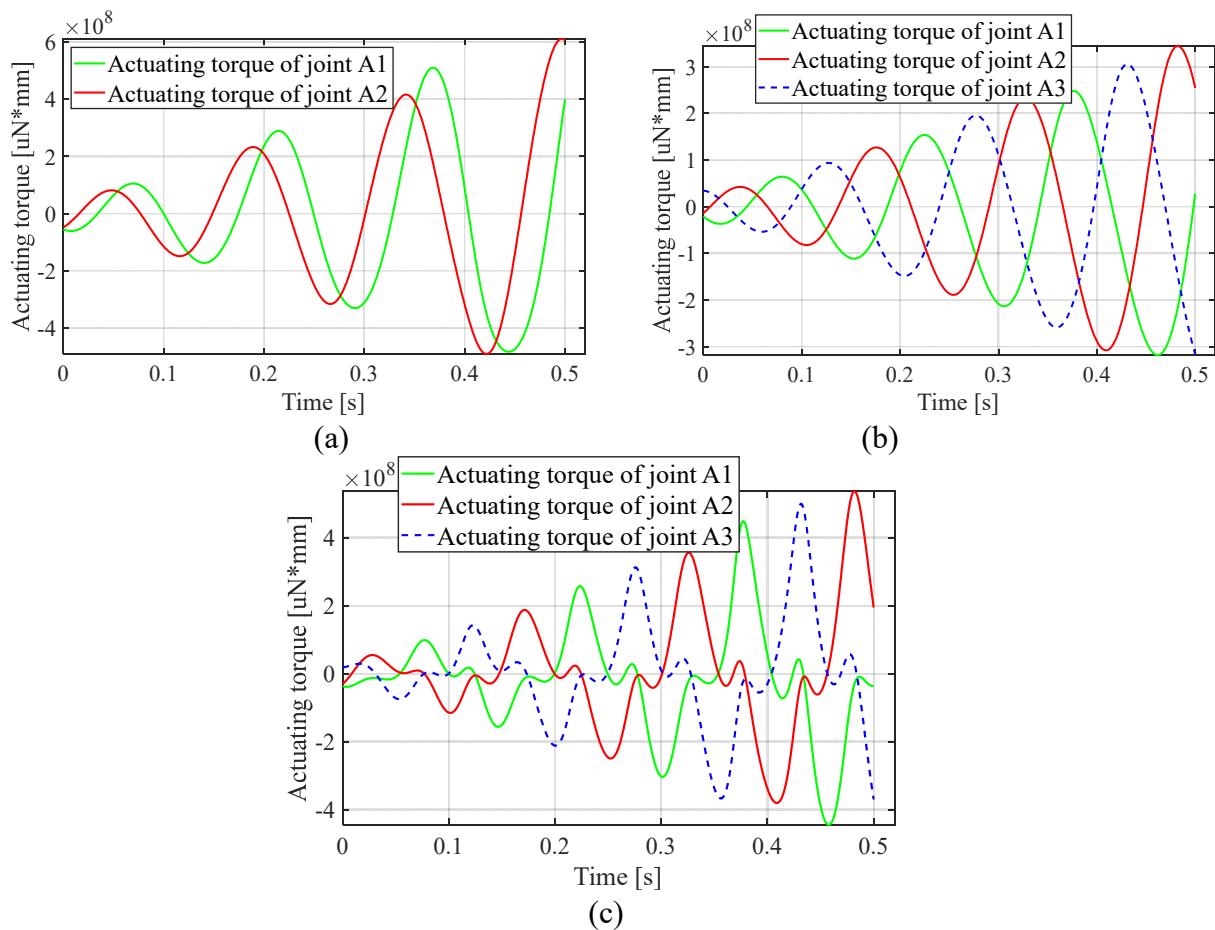


Figure 8. Three modes of feed-forward input torque of inverse rigid body dynamics: (a) non-redundant drive mode; (b) minimum Euclidean norm mode of internal force of redundant driving joint; (c) minimum Euclidean norm mode of active joint power.

When the end-effector moves in a planned trajectory, the driving torque has a unique solution for the non-redundant drive mode with two driving joints. However, for redundant drive mode with three driving joints, the distribution of driving torque is multi-solution. This study selected three types of driving torque distribution modes: (1) under non-redundant drive (A1, A2 are driving joints); (2) under redundant drive (A1, A2 and A3 are driving joints), the distribution of driving torque with minimum Euclidean norm of internal force of slave joints; (3) under redundant drive (A1, A2, A3 are driving joints), the distribution of driving torque with minimum European norm of driving joint power. The driving torque calculated via the inverse rigid body dynamic model (as shown in Figure 8) was used as the feed-forward input of the rigid-flexible coupling dynamic model to obtain the positive motion solution, thereby obtaining the dynamic response of the system.

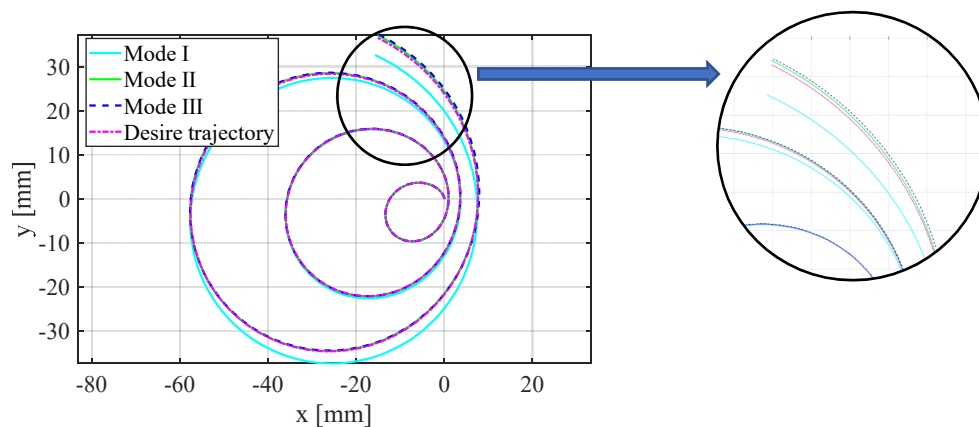


Figure 9. Trajectory of end-effector under the three driving torque distribution modes.

Figures 9 and 10 show that among the three modes, the trajectory of the end-effector is very close to the expected trajectory at the beginning, and the error increases gradually with the passage of time. In particular, the deviation of Mode 1 from the expected trajectory is relatively large at the final stage; this is more clearly observable in Figure 11. The redundant drive adopted in Modes 2 and 3 was found to effectively improve the dynamic performance of the parallel manipulator.

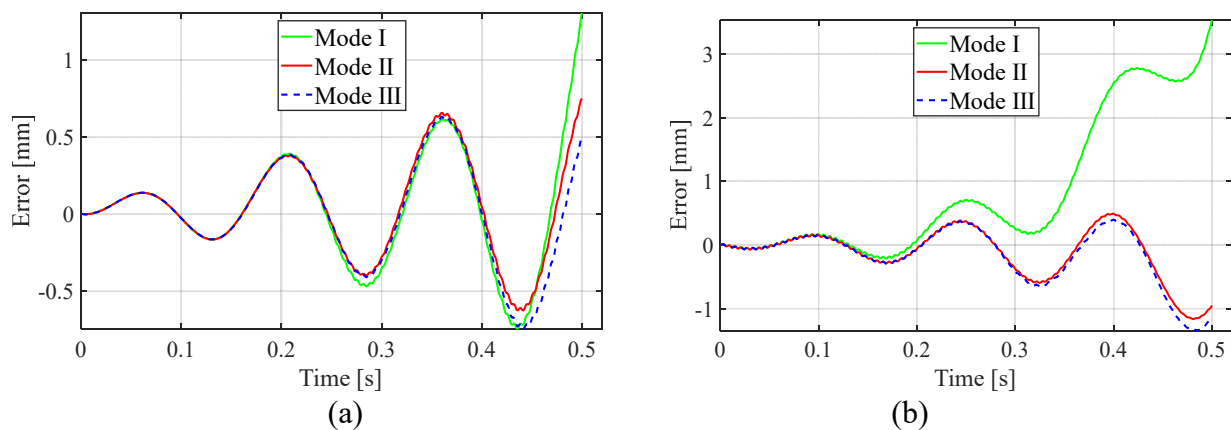


Figure 10. Motion error of end-effector under the three driving torque distribution modes: (a) x-direction error; (b) y-direction error.

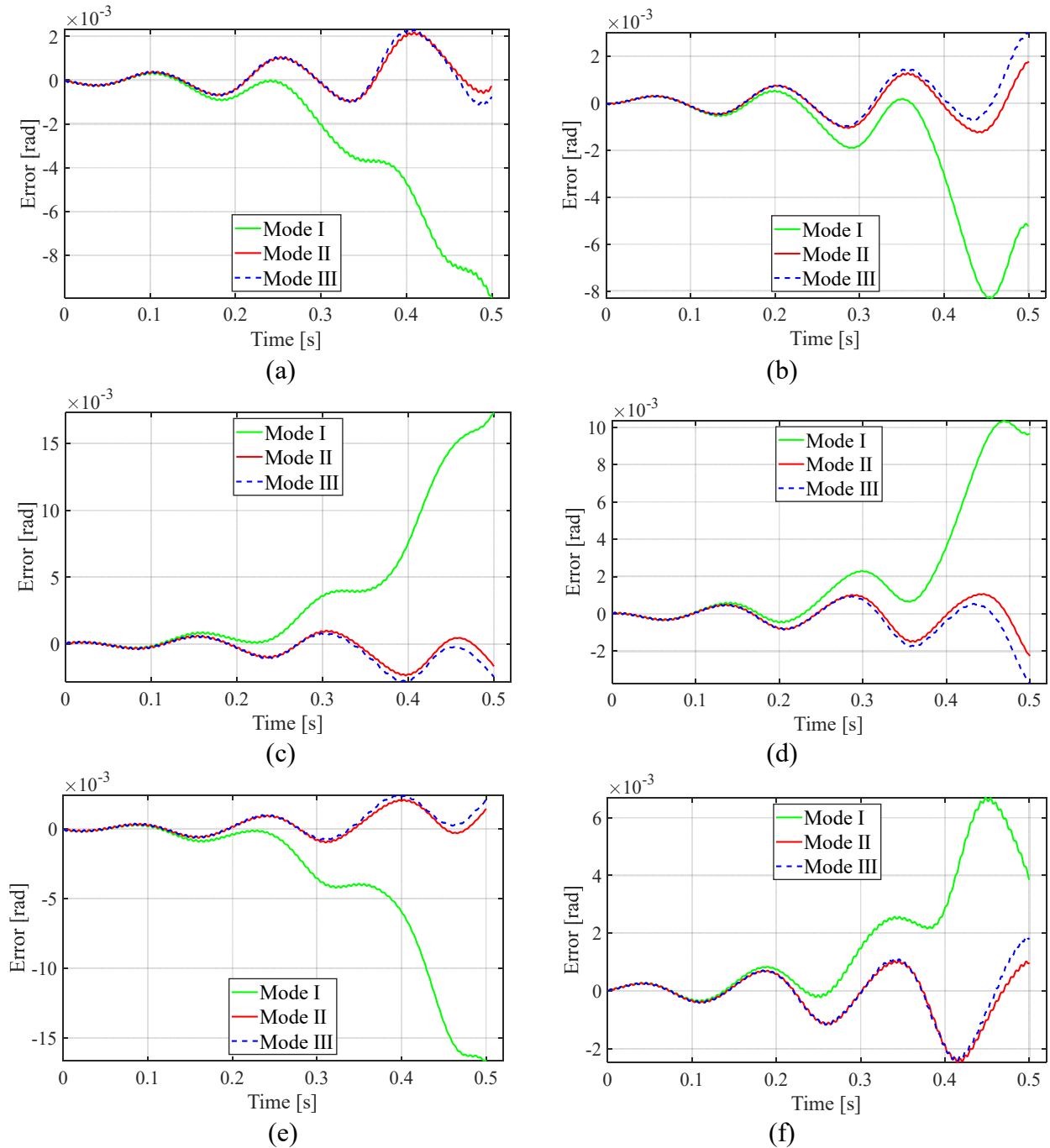


Figure 11. Angular error of three driving torque distribution modes. (a) angular error for Lever 1; (b) angular error for Lever 3; (c) angular error for Lever 5; (d) angular error for Lever 2; (e) angular error for Lever 4; (f) angular error for Lever 6.

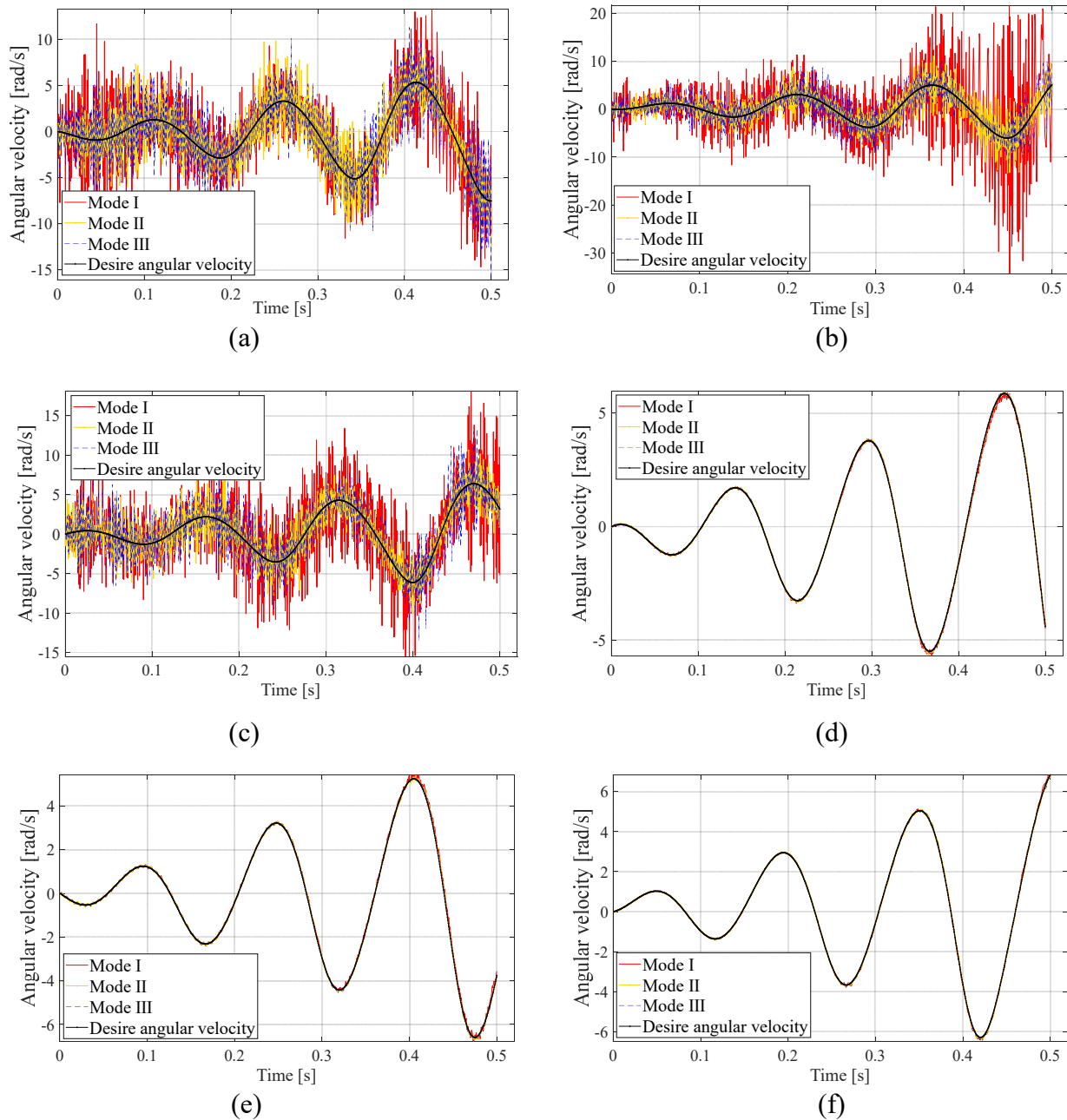


Figure 12. Angular velocity under three driving torque distribution modes. (a) Lever 1; (b) Lever 3; (c) Lever 5; (d) Lever 2; (e) Lever 4; (f) Lever 6.

Figures 12 and 13 show that the oscillation amplitude of angular velocity and angular acceleration of Levers 1, 3 and 5 is much larger than those of Levers 2, 4 and 6. This is because the former are flexible, while the latter are treated as rigid, and the oscillations generated by the latter are caused by the flexible body. In addition, the oscillation amplitude of Mode 1 is much larger than that of Modes 2 and 3, indicating that the dynamic performance of redundant drive is significantly better than that of the non-redundant drive, and the stability of the system driven by redundant drive is significantly improved.

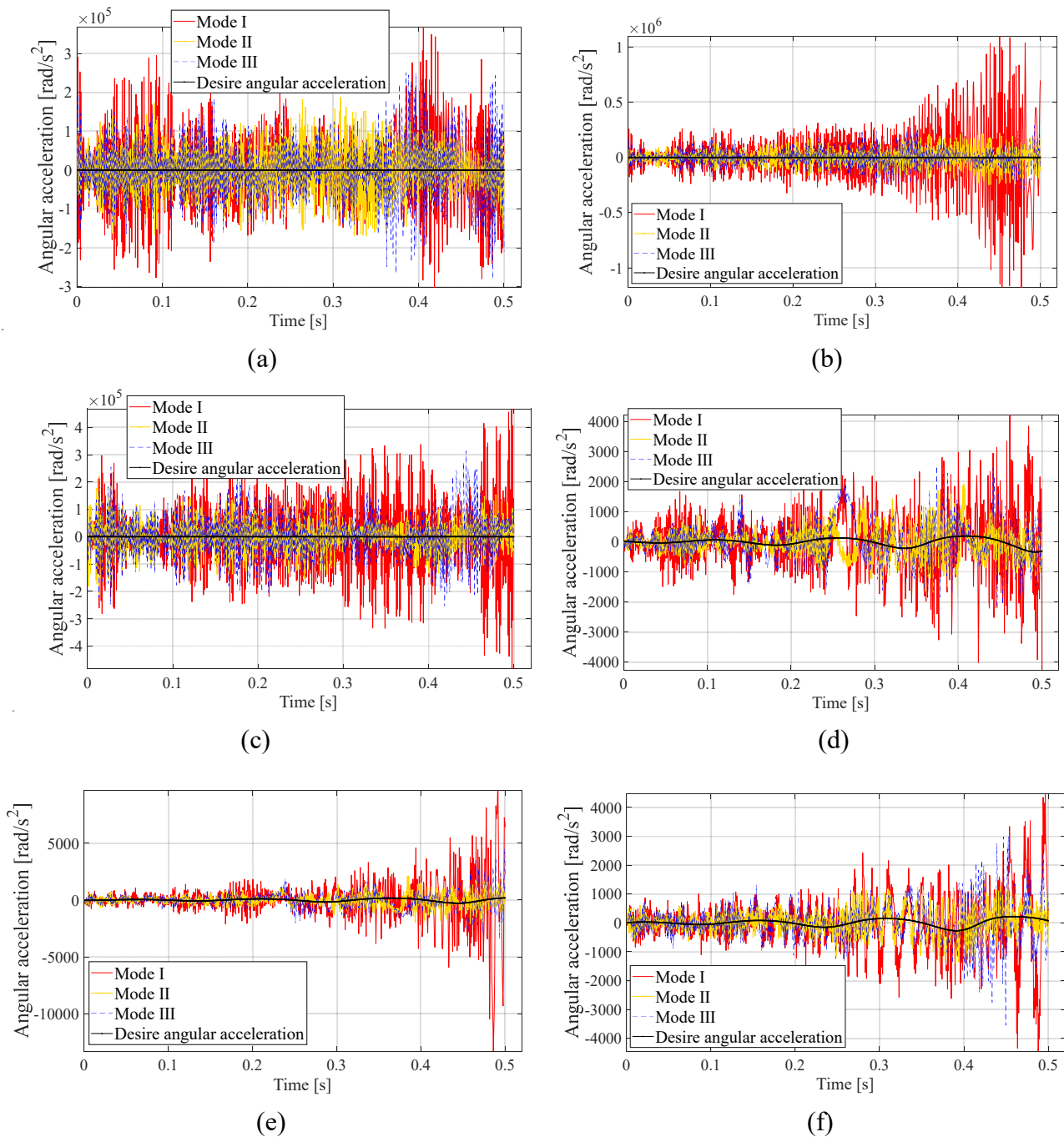


Figure 13. Angular acceleration under three driving torque distribution modes. (a) Lever 1; (b) Lever 3; (c) Lever 5; (d) Lever 2; (e) Lever 4; (f) Lever 6.

The elastic deformation at the end of the three flexible bodies can be clearly observed in Figures 14–16. The axial elastic deformation under the three modes is considerably small, i.e., three orders of magnitude smaller than the transverse deformation. Compared with the other two modes, Mode 2 exhibited smaller elastic deformation, more stable change, and better performance. The elastic deformation of Mode 1 in Figure 16 showed a significant decrease mainly owing to the non-redundant drive of Mode 1 and follower Lever 5.

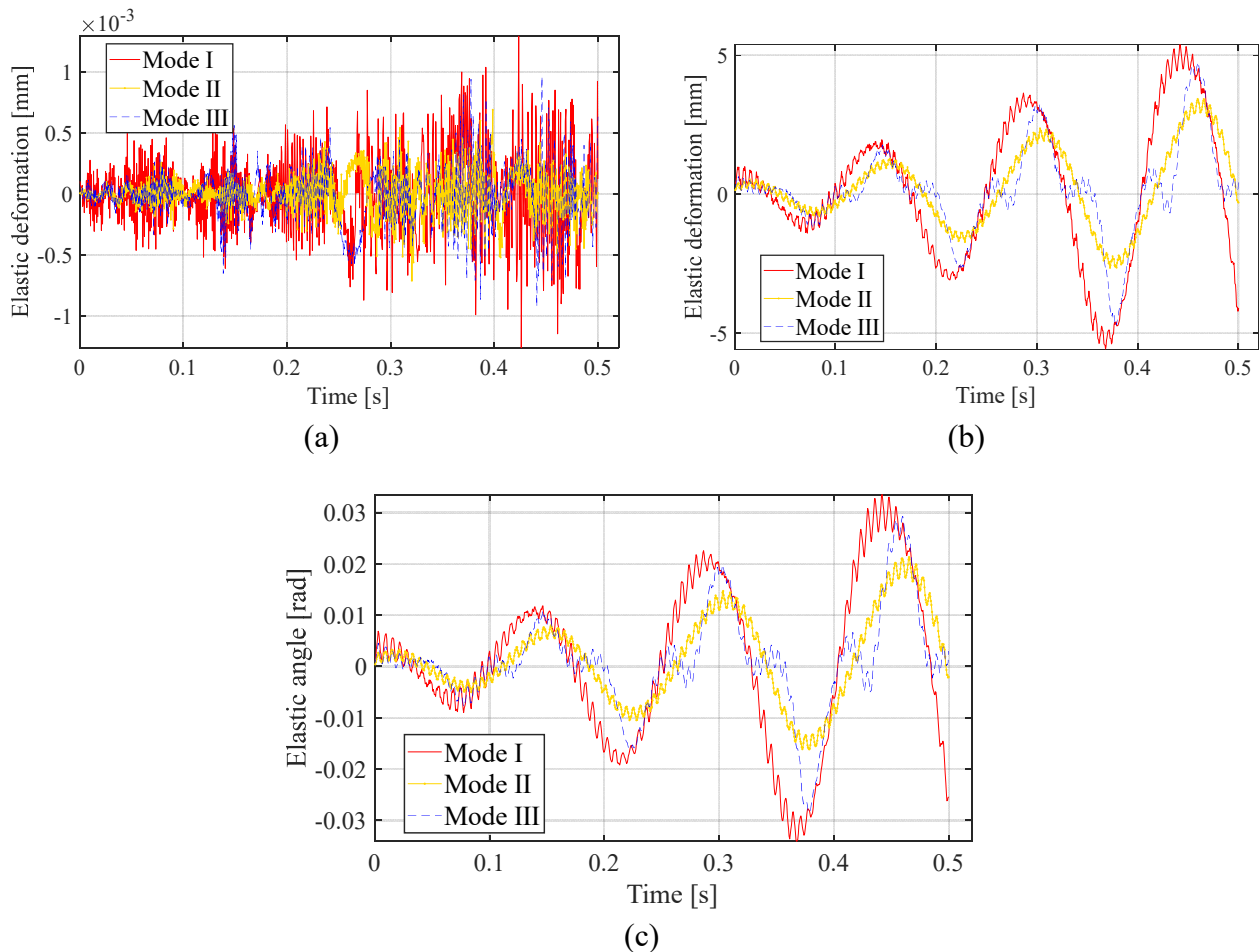


Figure 14. Elastic parameters of Lever 1 under three driving torque distribution modes: (a) axial deformation; (b) transverse deformation; (c) elastic angle.

5. Simulation verification

The simulation verification was based on the parametric model of the rigid-flexible coupling system of the 3-RRR parallel manipulator established on Adams. The modeling used a method similar to the finite segment discretization, wherein the three driving levers were discretized (Levers 1, 3 and 5), and each lever was divided into eight rigid segments linked by massless torsion springs (total of 24 segments). The three follower levers (Levers 2, 4 and 6) were not divided; the details are shown in the Figure 17. To facilitate the observation of the section of the lever, the parameters of Lever 1 were hidden and amplified, as shown in Figure 17(b). The driving torque under the previous Mode 2 was used as the feed-forward input of the simulation model, and certain simulation results were compared with the numerical model simulation results of the previous Mode 2, as shown in the Figures 18–21.

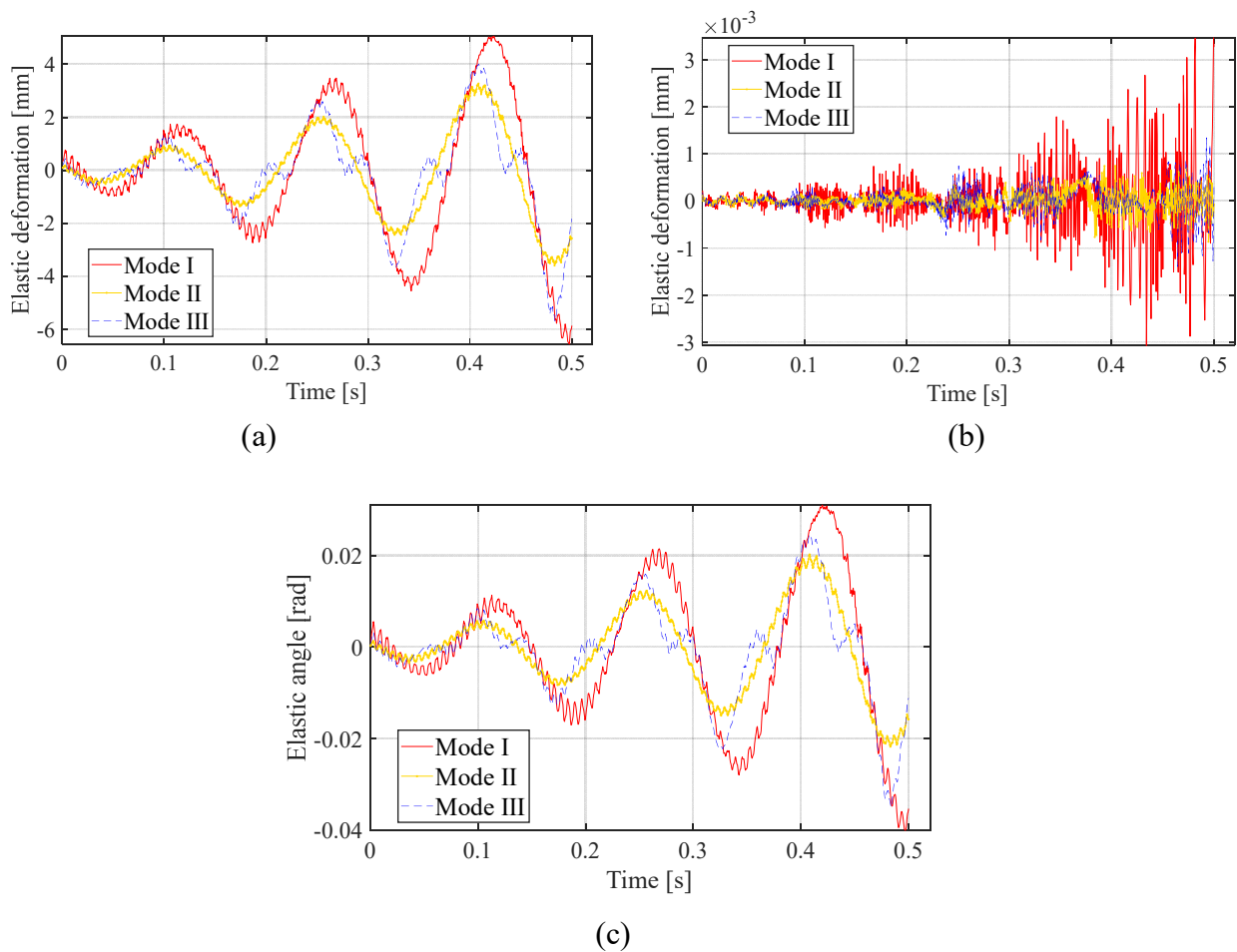


Figure 15. Elastic parameters of Lever 3 under three driving torque distribution modes: (a) axial deformation; (b) transverse deformation; (c) elastic angle.

To maintain generality, certain dynamic response parameters of the end-effector and each lever in Mode 2 were selected and compared with the simulation results. It was found that the trajectory and angular velocity of the end-effector in Figures 18 and 19 were nearly identical, and the velocity of the three follower levers in Figure 21 was consistent, with small deviations. Further, the velocity of the three driving levers in Figure 20 was consistent in general, with certain deviations. This is mainly because the discretization technology used in the two methods is different. The numerical simulation uses FEM while the software simulation uses FSM. Thus, it was confirmed that the rigid-flexible coupling dynamic model established in this study is accurate.

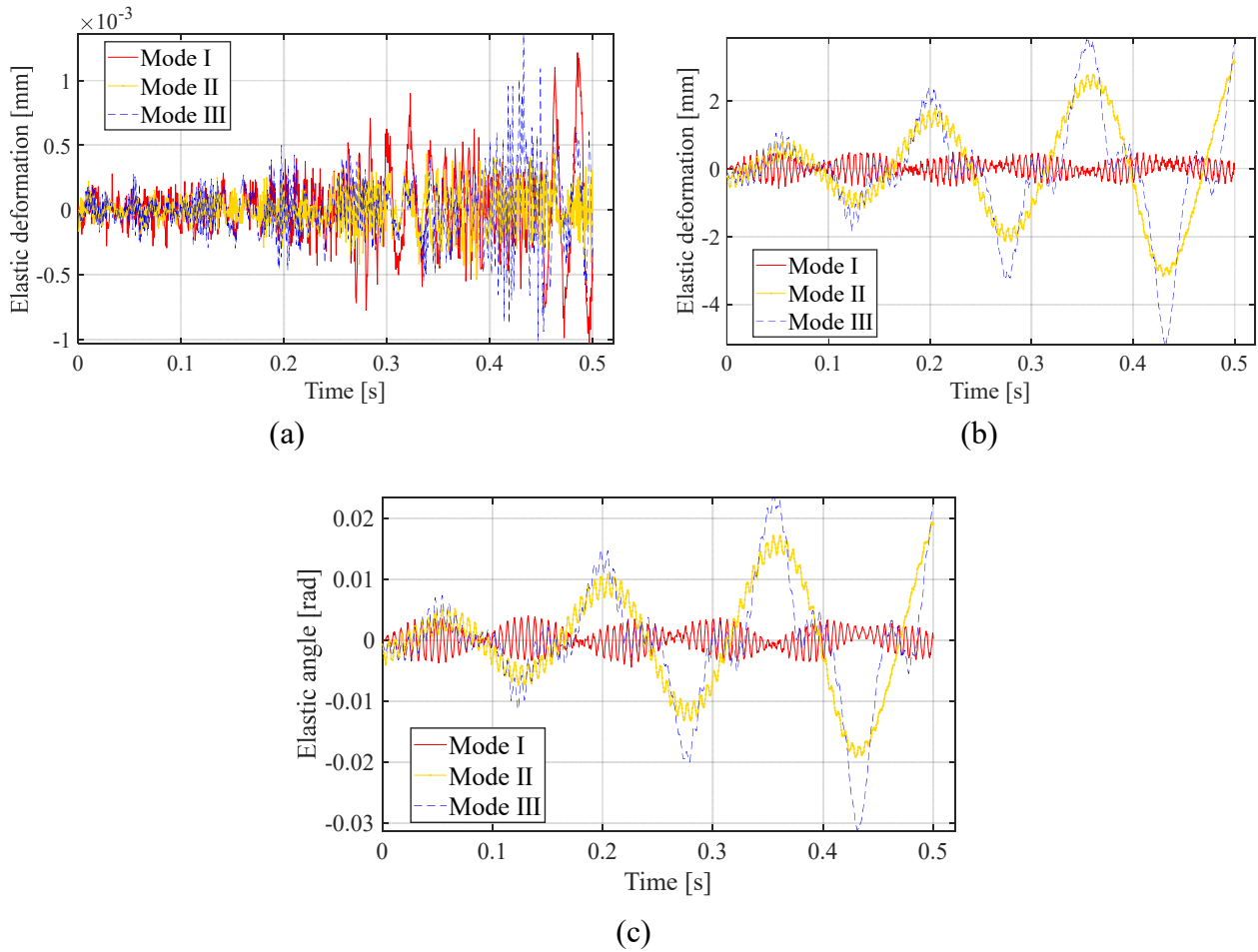


Figure 16. Elastic parameters of Lever 5 under three driving torque distribution modes: (a) axial deformation; (b) transverse deformation; (c) elastic angle.

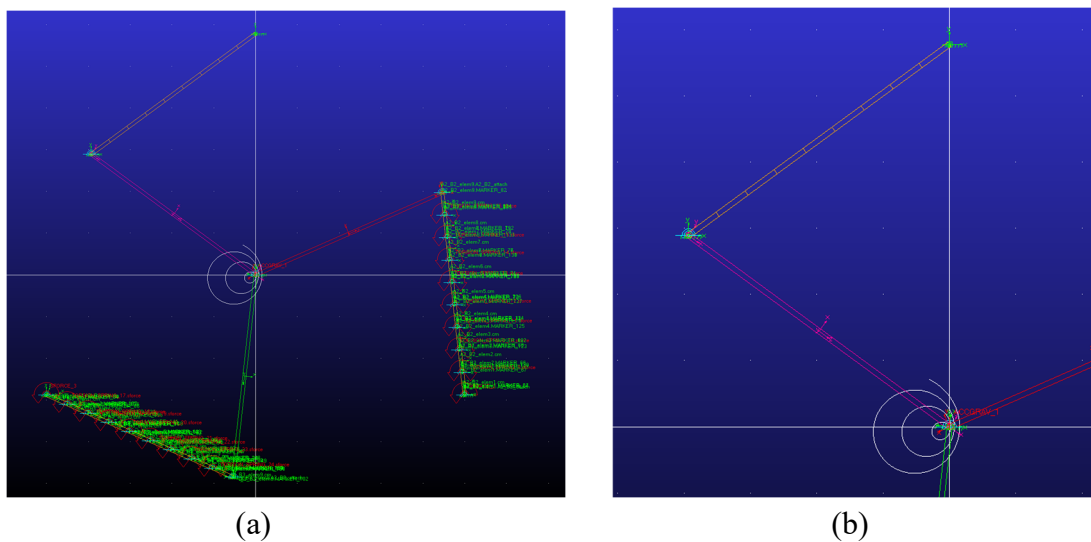


Figure 17. Adams simulation model and trajectory.

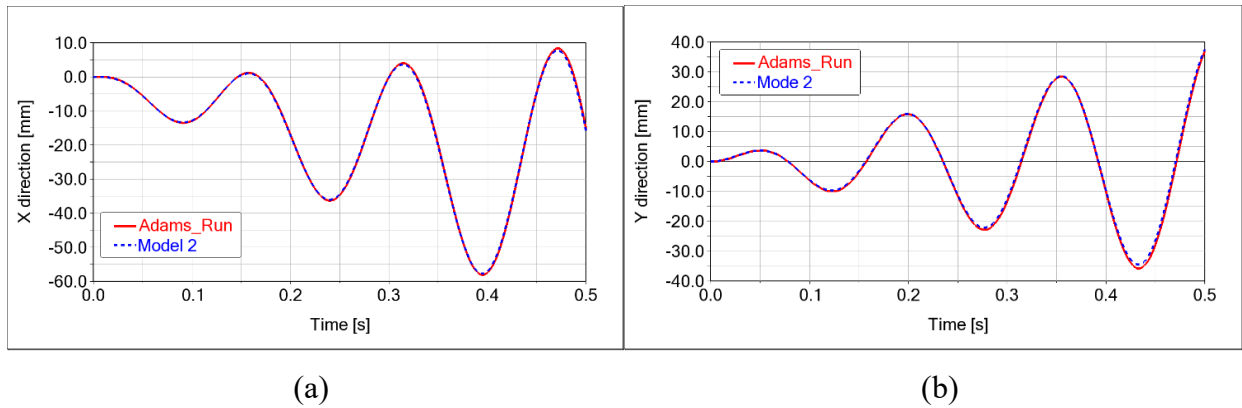


Figure 18. (a) Displacement of the end effector in x-direction; (b) Displacement of the end effector in y-direction.

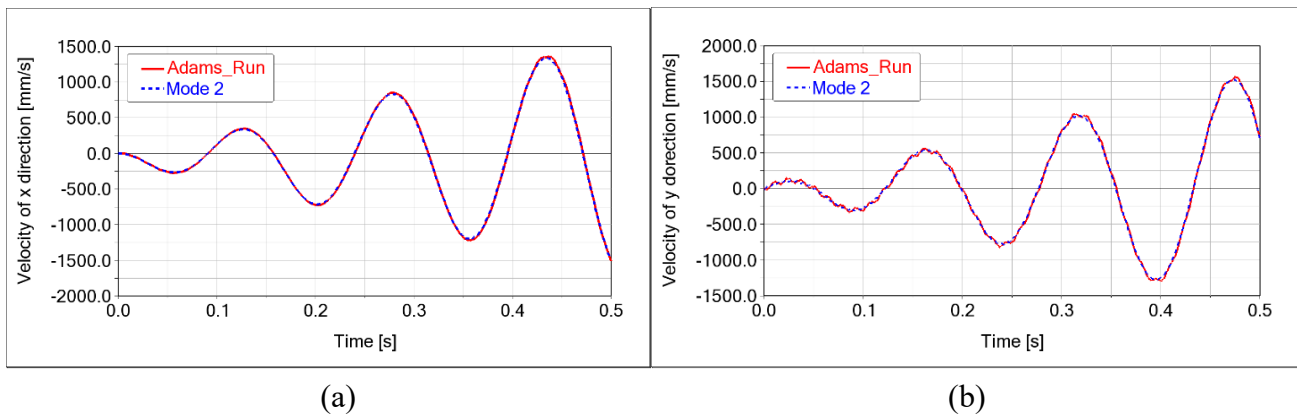


Figure 19. (a) Velocity of end-effector in x-direction; (b) Velocity of end-effector in y-direction.

6. Conclusions

This study determined the configuration of 3-RRR parallel manipulator and performed a flexible treatment to establish a rigid-flexible coupling dynamic model. The modular modeling method is conducive for extension to other models and soft programming. The dynamic response of three different driving torque distribution modes was obtained via numerical simulation. Finally, FSM was used to establish the model in Adams, and the established model was verified. The conclusions of this study are as follows:

(1) Establishing dynamics model of flexible link system

The rod was finitely discretized by the element method, and the dynamic equation of the module was established using the floating reference coordinate system. Further, the module was linked to establish the dynamic equation of the flexible body. All the flexible bodies were combined to obtain the dynamic equation of the open chain system, and a complete system dynamics equation was established. The modular modeling method was applied in the entire process. First, the independent flexible body dynamics equation was established. Second, based on the constraint equation, each segment was grouped together to form a complete equation, which is conducive to the promotion of

other modeling and software programming systems, as well as lightweight design and system dynamic performance optimization.

(2) Numerical simulation and analysis

The driving torque in the three modes obtained by inverse rigid body dynamics was used as the feed-forward input of numerical simulation to obtain the dynamic response using the ode23tb solver. The analysis revealed that the redundant drive had better dynamic performance than the non-redundant drive and exhibited a suitable inhibitory effect on vibration. In addition, the dynamic performance of Mode 2 was smoother, with smaller vibration, compared to that of Mode 3. From the flexible deformation perspective, the axial deformation was much smaller than the transverse deformation, and they differed by three orders of magnitude. Moreover, the deformation of the driven flexible body was smaller than that of the active flexible body. Furthermore, the deformation of driving lever in Mode 2 was smaller than that in Modes 1 and 3, and the change was more stable with the performance being better than the other two modes.

(3) Finally, FSM was used to establish the simulation model in Adams.

The driving torque of Mode 2 is selected as the feed-forward input, and certain dynamic response results were compared with the numerical simulation results to verify the correctness of the established rigid-flexible coupling dynamic model.

This paper mainly carries out the dynamic modeling and dynamic analysis of flexible Lever parallel robots. It will be carried out around the control strategy of parallel robots in the follow-up research, which improve its trajectory tracking and positioning accuracy, the potential application fields of the parallel robot including fast packaging, fast sorting, high-speed motion simulation, etc.

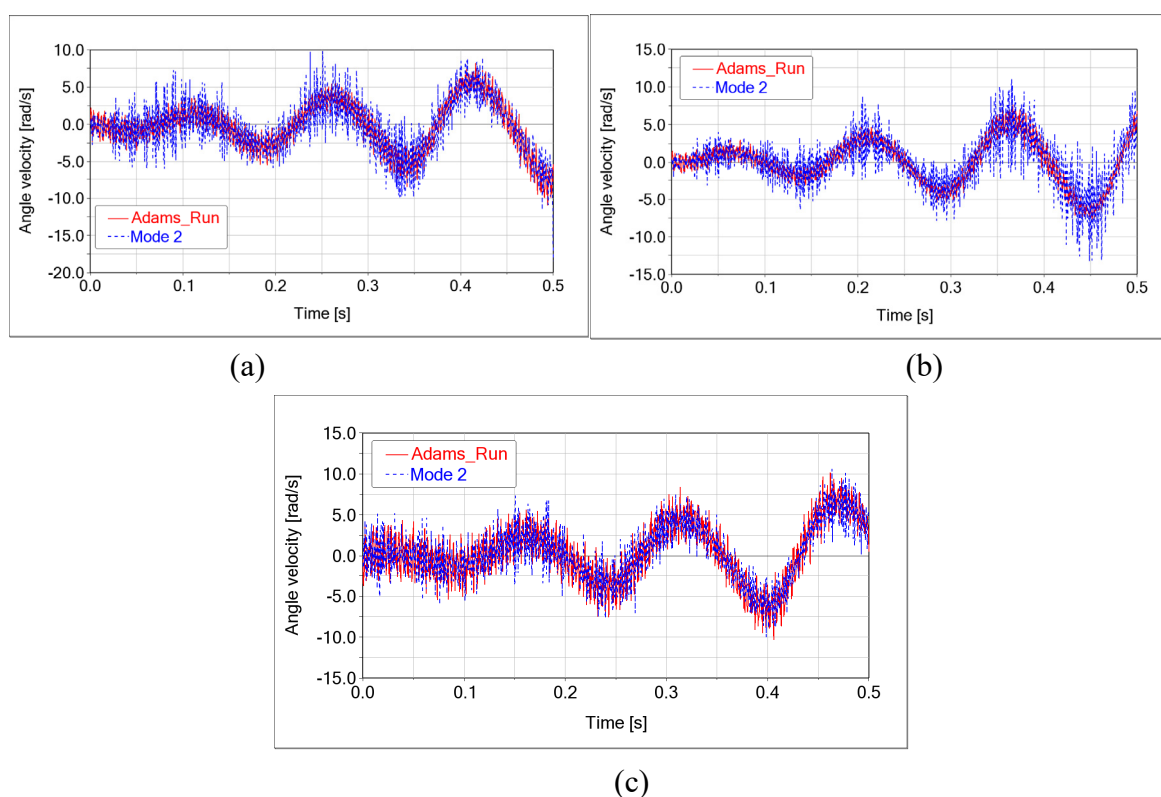


Figure 20. Angular velocity of three flexible driving levers: (a) Lever 1; (b) Lever 3; (c) Lever 5.

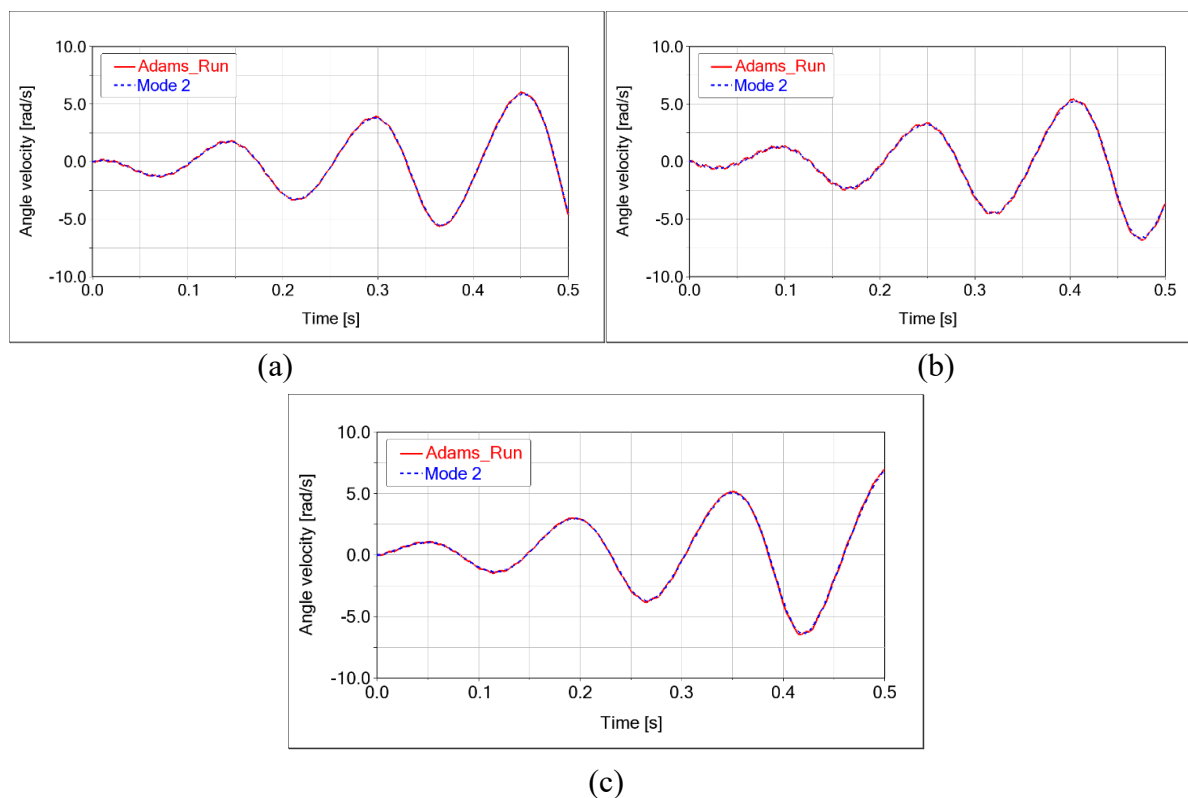


Figure 21. Angular velocity of three rigid follower levers: (a) Lever 2; (b) Lever 4; (c) Lever 6.

Acknowledgments

The authors would like to appreciate the editors and the reviewers for their significant contributions to the improvement of the paper. Thanks to Xi'an Jiaotong University for their help in this study. In this paper, the MATLAB calculations and ADAMS dynamics simulations are completed in Xi'an Jiaotong University.

Conflict of interest

The authors declare that they have no conflict of interest.

References

1. C. Gosselin, J. Angeles, Singularity analysis of closed-loop kinematic chains, *IEEE Trans. Rob. Automat*, **6** (1990), 281–290. <https://doi.org/10.1109/70.56660>
2. H. Ye, D. Wang, J. Wu, Y. Yue, Y. Zhou, Forward and inverse kinematics of a 5-DOF hybrid robot for composite material machining, *Rob. Comput. Integr. Manuf.*, **65** (2020), 101961. <https://doi.org/10.1016/j.rcim.2020.101961>
3. K. Dong, D. Li, X. Xue, C. Xu, H. Wang, X. Gao, Workspace and accuracy analysis on a novel 6-UCU bone-attached parallel manipulator, *Chin. J. Mech. Eng.*, **35** (2022), 35. <https://doi.org/10.1186/s10033-022-00689-1>

4. P. Yan, H. Huang, B. Li, D. Zhou, A 5-DOF redundantly actuated parallel mechanism for large tilting five-face machining, *Mech. Mach. Theory*, **172** (2022), 104785. <https://doi.org/10.1016/j.mechmachtheory.2022.104785>
5. B. Ren, Z. Zhang, Design of 4PUS-PPPS redundant parallel mechanism oriented to the visual system of flight simulator, *Int. J. Intell. Robot. Appl.*, **5** (2021), 534–542. <https://doi.org/10.1007/s41315-021-00210-2>
6. T. Liu, Y. Hu, H. Xu, Z. Zhang, H. Li, Investigation of the vectored thruster AUVs based on 3SPS-S parallel manipulator, *Appl. Ocean Res.*, **85** (2019), 151–161. <https://doi.org/10.1016/j.apor.2019.01.025>
7. M. Arsenault, R. Boudreau, The synthesis of three-degree-of-freedom planar parallel mechanisms with revolute joints (3-RRR) for an optimal singularity-free workspace, *J. Robot. Syst.*, **21** (2004), 259–274. <https://doi.org/10.1002/rob.20013>
8. A. K. Dash, I. M. Chen, S. H. Yeo, G. Yang, Workspace generation and planning singularity-free path for parallel manipulators, *Mech. Mach. Theory*, **40** (2005), 776–805. <https://doi.org/10.1016/j.mechmachtheory.2005.01.001>
9. A. G. Ruiz, J. C. Santos, J. Croes, W. Desmet, M. M. da Silva, On redundancy resolution and energy consumption of kinematically redundant planar parallel manipulators, *Robotica*, **36** (2018), 809–821. <https://doi.org/10.1017/S026357471800005X>
10. N. Baron, A. Philippides, N. Rojas, A novel kinematically redundant planar parallel robot manipulator with full rotatability, *J. Mech. Robot.*, **11** (2019), 011008. <https://doi.org/10.1115/1.4041698>
11. C. Cheng, W. Xu, J. Shang, Optimal distribution of the actuating torques for a redundantly actuated masticatory robot with two higher kinematic pairs, *Nonlinear Dyn.*, **79** (2015), 1235–1255. <https://doi.org/10.1007/s11071-014-1739-9>
12. D. Liang, Y. Song, T. Sun, X. Jin, Dynamic modeling and hierarchical compound control of a novel 2-DOF flexible parallel manipulator with multiple actuation modes, *Mech. Syst. Signal Process.*, **103** (2018), 413–439. <https://doi.org/10.1016/j.ymsp.2017.10.004>
13. D. Liang, Y. Song, T. Sun, X. Jin, Rigid-flexible coupling dynamic modeling and investigation of a redundantly actuated parallel manipulator with multiple actuation modes, *J. Sound Vibration*, **403** (2017), 129–151. <https://doi.org/10.1016/j.jsv.2017.05.022>
14. Z. Chen, M. Kong, C. Ji, M. Liu, An efficient dynamic modelling approach for high-speed planar parallel manipulator with flexible links, *Proc. Inst. Mech. Eng. Part C*, **229** (2015), 663–678. <https://doi.org/10.1177/0954406214538946>
15. A. Rosyid, B. El-Khasawneh, Multibody dynamics of nonsymmetric planar 3PRR parallel manipulator with fully flexible links, *Appl. Sci.*, **10** (2020), 4816. <https://doi.org/10.3390/app10144816>
16. L. Sheng, W. Li, Y. Wang, M. Fan, X. Yang, Dynamic model and vibration characteristics of planar 3-RRR parallel manipulator with flexible intermediate links considering exact boundary conditions, *Shock Vibration*, **2017** (2017), 1–13. <https://doi.org/10.1155/2017/1582547>
17. M. Burkhardt, R. Seifried, P. Eberhard, Experimental studies of control concepts for a parallel manipulator with flexible links, *J. Mech. Sci. Technol.*, **29** (2015), 2685–2691. <https://doi.org/10.1007/s12206-015-0515-1>

18. M. Morlock, N. Meyer, M. A. Pick, R. Seifried, Real-time trajectory tracking control of a parallel robot with flexible links, *Mech. Mach. Theory*, **158** (2021), 104220. <https://doi.org/10.1016/j.mechmachtheory.2020.104220>
19. F. T. Colombo, M. M. da Silva, Two hybrid model-based control strategies for a flexible parallel planar manipulator, *Control Eng. Pract.*, **127** (2022), 105306. <https://doi.org/10.1016/j.conengprac.2022.105306>
20. S. Karande, P. S. V. Nataraj, P. S. Gandhi, M. M. Deshpande, Control of parallel flexible five bar manipulator using QFT, in *2009 IEEE International Conference on Industrial Technology*, **2009** (2009), 1–6. <https://doi.org/10.1109/ICIT.2009.4939693>
21. X. Wang, J. K. Mills, FEM dynamic model for active vibration control of flexible linkages and its application to a planar parallel manipulator, *Appl. Acoust.*, **66** (2005), 1151–1161. <https://doi.org/10.1016/j.apacoust.2005.02.009>
22. V. Sonneville, A. Cardona, O. Bruls, Geometrically exact beam finite element formulated on the special Euclidean group, *Comput. Methods Appl. Mech. Eng.*, **268** (2014), 451–474. <https://doi.org/10.1016/j.cma.2013.10.008>
23. G. P. Cai, C.W. Lim, Dynamics studies of a flexible hub–beam system with significant damping effect, *J. Sound Vibration*, **318** (2008), 1–17. <https://doi.org/10.1016/j.jsv.2008.06.009>
24. E. Mirzaee, M. Eghtesad, S. A. Fazelzadeh, Maneuver control and active vibration suppression of a two-link flexible arm using a hybrid variable structure/Lyapunov control design, *Acta Astronaut.*, **67** (2010), 1218–1232. <https://doi.org/10.1016/j.actaastro.2010.06.054>
25. M. Dupac, D. G. Beale, Dynamic analysis of a flexible linkage mechanism with cracks and clearance, *Mech. Mach. Theory*, **45** (2010), 1909–1923. <https://doi.org/10.1016/j.mechmachtheory.2010.07.006>
26. S. Šalinić, An improved variant of Hencky bar-chain model for buckling and bending vibration of beams with end masses and springs, *Mech. Syst. Signal Process.*, **90** (2017), 30–43. <https://doi.org/10.1016/j.ymsp.2016.12.007>
27. R. J. Theodore, A. Ghosal, Comparison of the assumed modes and finite element models for flexible multilink manipulators, *Int. J. Rob. Res.*, **14** (1995), 91–111. <https://doi.org/10.1177/027836499501400201>
28. W. Shang, S. Cong, Nonlinear adaptive task space control for a 2-DOF redundantly actuated parallel manipulator, *Nonlinear Dyn.*, **59** (2010), 61–72. <https://doi.org/10.1007/s11071-009-9520-1>
29. A. Shabana, *Vibration of Discrete and Continuous Systems*, Springer International Publishing, Cham, 2019. <https://doi.org/10.1007/978-3-030-04348-3>



AIMS Press

©2023 the Author(s), licensee AIMS Press. This is an open access article distributed under the terms of the Creative Commons Attribution License (<http://creativecommons.org/licenses/by/4.0>)